

¹ **Whole-brain comparison of rodent and human brains
2 using spatial transcriptomics**

³

⁴ Antoine Beauchamp^{1,2,3,*}, Yohan Yee^{1,2,3}, Ben C. Darwin^{1,2}, Armin Raznahan⁴, Rogier B.
⁵ Mars^{5,6,†}, Jason P. Lerch^{1,2,3,5,*†}

⁶

⁷ ¹Mouse Imaging Centre, Toronto, Ontario, Canada.

⁸ ²The Hospital for Sick Children, Toronto, Ontario, Canada.

⁹ ³Department of Medical Biophysics, University of Toronto, Toronto, Ontario, Canada.

¹⁰ ⁴Section on Developmental Neurogenomics, Human Genetics Branch, National Institute of Mental Health Intramural
¹¹ Research Program, Bethesda, MD, U.S.A.

¹² ⁵Wellcome Centre for Integrative Neuroimaging, Centre for Functional MRI of the Brain (FMRIB), Nuffield Depart-
¹³ ment of Clinical Neurosciences, John Radcliffe Hospital, University of Oxford, Oxford, United Kingdom.

¹⁴ ⁶Donders Institute for Brain, Cognition and Behaviour, Radboud University Nijmegen, Nijmegen, Netherlands.

¹⁵ [†]These authors contributed equally to this work.

¹⁶ *Corresponding author. Email: antoine.beauchamp@mail.utoronto.ca (A.B.); jason.lerch@ndcn.ox.ac.uk (J.P.L)

¹⁷ **Abstract**

¹⁸ The ever-increasing use of mouse models in preclinical neuroscience research calls for an improvement in the
¹⁹ methods used to translate findings between mouse and human brains. Previously we showed that the brains
²⁰ of primates can be compared in a direct quantitative manner using a common reference space built from
²¹ white matter tractography data (Rogier B. Mars et al., 2018b). Here we extend the common space approach
²² to evaluate the similarity of mouse and human brain regions using openly accessible brain-wide transcrip-
²³ tomic data sets. We show that mouse-human homologous genes capture broad patterns of neuroanatomical
²⁴ organization, but that the resolution of cross-species correspondences can be improved using a novel su-
²⁵ pervised machine learning approach. Using this method, we demonstrate that sensorimotor subdivisions of
²⁶ the isocortex exhibit greater similarity between species, compared with supramodal subdivisions, and that
²⁷ mouse isocortical regions separate into sensorimotor and supramodal clusters based on their similarity to
²⁸ human cortical regions. We also find that mouse and human striatal regions are strongly conserved, with
²⁹ the mouse caudoputamen exhibiting an equal degree of similarity to both the human caudate and putamen.

30 Introduction

31 Animal models play an indispensable role in neuroscience research, not only for understanding disease and
32 developing treatments, but also for obtaining data that cannot be obtained in the human. While numerous
33 species have been used to model the human brain, the mouse has emerged as the most prominent of these,
34 due to its rapid life cycle, straightforward husbandry, and amenability to genetic engineering (Dietrich et
35 al., 2014; Ellenbroek and Youn, 2016; Hedrich et al., 2004; Houdebine, 2004). Mouse models have proven
36 to be extremely useful for understanding diverse features of the brain, from its molecular neurobiological
37 properties to its large-scale network properties (Hodge et al., 2019; Oh et al., 2014; Yao et al., 2021).
38 However, translating findings from the mouse to the human has not been straightforward. This is especially
39 evident in the context of neuropsychopharmacology, where promising neuropsychiatric drugs have one of the
40 highest failures rates in Phase III clinical trials (Hay et al., 2014).

41 Successful translation requires an understanding of how effects on the brain of the model species are likely to
42 manifest in the brain of the actual species of interest. This is not trivial in the case of the mouse and human,
43 as the two species diverged from a common ancestor about 80 million years ago (Kaas, 2012). Although
44 common themes are apparent in the brains of all mammalian species studied to date (Krubitzer, 2007), there
45 remain substantial differences between the mouse and human brain. Beyond the obvious differences in size,
46 large parts of the human cortex potentially have no corresponding homologues in the mouse (Preuss, 1995).
47 Direct comparisons across the brains of different species are further complicated by the fact that researchers
48 from different traditions use inconsistent nomenclature to refer to similar neuroanatomical areas (Heukelum
49 et al., 2020; Laubach et al., 2018).

50 Over the course of the last decade, we have developed novel approaches to explicitly evaluate similarities
51 and differences between the brains of related species. These approaches describe brains using common data
52 spaces that are directly comparable between species, making it possible to evaluate the similarity of different
53 regions in a quantitative fashion (Mars et al., 2021). This way, potential homologues can be formally tested
54 and regions of the brain that do not allow for straightforward translation can be identified (Rogier B. Mars
55 et al., 2018b). Establishing such a formal translation between the mouse and the human brain would allow
56 scientists involved in translational research to explicitly test hypotheses about conservation of brain regions,
57 identify regions that are well suited to translational paradigms, and directly transform quantitative maps
58 from the brain of one species to the other.

59 One approach towards building these common spaces has been to exploit connectivity. It has previously
60 been demonstrated that brain regions can be identified via their unique set of connections to other regions

61 in the brain. This *connectivity fingerprint* can therefore be seen as a diagnostic of an area (Rogier B. Mars
62 et al., 2018a; Passingham et al., 2002). The common connectivity space approach relies on defining agreed
63 upon neuroanatomical homologues *a priori* and then expressing the connectivity fingerprint of regions under
64 investigation with those established homologues in the two brains (Mars et al., 2016b). The connections
65 of any given region to the established homologues thus form a common space, which links the two brains.
66 In a series of early studies, we compared the connectivity of the macaque and human brain, identifying
67 homologies as well as specializations across association cortex (Mars et al., 2013; Neubert et al., 2014; Sallet
68 et al., 2013). The same approach has recently been applied to mouse-human comparisons for the first time,
69 demonstrating conserved organization between the mouse and human striatum, but some specialization in
70 the human caudate related to connectivity with the prefrontal cortex (Balsters et al., 2020). A similar study
71 recently compared connectivity of the medial frontal cortex across rats, marmosets, and humans (Schaeffer et
72 al., 2020). However, the lack of established neuroanatomical homologues in mice, particularly in the cortex,
73 limits the use of connectivity to compare these species.

74 A more promising approach to mouse-human comparisons could be to exploit the spatial patterns of gene
75 expression. Advances in transcriptomic mapping can be used to characterise the differential expression of
76 many thousands of genes across the brain and compare the pattern between regions (Ortiz et al., 2020).
77 Moreover, the availability of whole-brain spatial transcriptomic data sets for multiple species provides an
78 opportunity to run novel analyses at low cost (Hawrylycz et al., 2012; Lein et al., 2007). Such maps for the
79 human cortex show topographic patterns that mimic those observed in other modalities, such as a gradient
80 between primary and heteromodal areas of the neocortex (Burt et al., 2018). Importantly, these patterns
81 appear to be conserved across mammalian species (Fulcher et al., 2019), which opens up the possibility
82 of using the expression of homologous genes as a common space across species. In fact, a recent study
83 demonstrated how the expression of homologous genes can be used to directly register mouse and vole brains
84 into a common reference frame, which allows for direct point-by-point comparisons of brain maps (Englund
85 et al., 2021). However, this specific approach is only feasible because of the large degree of morphological
86 similarity between mouse and vole brains. In the case of mouse-human comparisons, we almost certainly
87 cannot directly register mouse and human brains into a common coordinate frame using methods for image
88 registration. Hence we need to be more creative in our approach.

89 Here we examine the patterns of similarity between the mouse and human brain using a common space
90 constructed from spatial gene expression data sets. We begin with an initial set of 2835 homologous genes.
91 Subsequently, we present and evaluate a novel method for improving the resolution of mouse-human neu-
92 roanatomical correspondences using a supervised machine learning approach. Using the novel representation

93 of the gene expression common space, i.e. a latent gene expression space, we analyse the similarity of mouse
94 and human isocortical subdivisions and demonstrate that sensorimotor regions exhibit a higher degree of sim-
95 ilarity than supramodal regions. Finally, we examine the patterns of transcriptomic similarity at a voxel-wise
96 level in the mouse and human striatum.

97 Results

98 Homologous genes capture broad similarities in the mouse and human brains

99 We first examined the pattern of similarities that emerged when comparing mouse and human brain regions
100 on the basis of their gene expression profiles. We constructed a gene expression common space using widely
101 available data sets from the Allen Institute for Brain Science: the Allen Mouse Brain Atlas (AMBA) and
102 the Allen Human Brain Atlas (AHBA) (Hawrylycz et al., 2012; Lein et al., 2007). These data sets provide
103 whole-brain coverage of expression intensity for thousands of genes in the mouse and human genomes. For
104 our purposes we filtered these gene sets to retain only mouse-human homologous genes using a list of ortho-
105 logues obtained from the NCBI HomoloGene system (NCBI 2018). Using a gene enrichment analysis, we
106 found that this reduced gene set was significantly associated with a number of biological processes related to
107 the nervous system, with Gene Ontology labels such as “nervous system development”, “neurogenesis”, and
108 “regulation of nervous system development”. Additional modules returned with high significance were “reg-
109 ulation of multicellular organismal process”, “regulation of biological quality”, and “multicellular organism
110 development”. The full set of significant modules can be found in Supplementary File 1.

111 Prior to analysis, the mouse and human homologous gene expression data sets were pre-processed using a
112 pipeline that included quality control checks, normalization procedures, and aggregation of the expression
113 values under a set of atlas labels. The result was a gene-by-region matrix in either species, describing the
114 normalized expression of 2835 homologous genes across 67 mouse regions and 88 human regions (see Materials
115 and methods). We quantified the degree of similarity between all pairs of mouse and human regions using
116 the Pearson correlation coefficient, resulting in a mouse-human similarity matrix (Figure 1A).

117 We find that the similarity matrix exhibits broad patterns of positive correlation between the mouse and
118 human brains. These clusters of similarity correspond to coarse neuroanatomical regions that are generally
119 well-defined in both species. For instance, we observe that, overall, the mouse isocortex is similar to the
120 human cerebral cortex, with the exception of the hippocampal formation, which forms a unique cluster.
121 Similarly the mouse and human cerebellar hemispheres cluster together, while the cerebellar nuclei show

122 relatively high correlation to each other ($r = 0.351$) as well as to brain stem structures like the pons
123 ($r = 0.328$ and $r = 0.335$ for the mouse and human nuclei respectively) and myelencephalon ($r = 0.288$ and
124 $r = 0.351$). The associations between broad regions such as these are self-evident in the correlation matrix.

125 Our ability to resolve regional matches on a finer scale is limited when using all homologous genes in this way.
126 This is especially true for regions within the cerebral and cerebellar cortices, which exhibit a high degree
127 of internal homogeneity. This is apparent in the similarity profiles, defined here as the set of correlation
128 values between a given seed region and all target regions in the other species. For example, the human
129 precentral gyrus and cuneus are most strongly correlated to many regions of the mouse isocortex. While
130 the brain maps feature a rostral-caudal gradient (Figure 1B), the profiles of the two seeds are highly similar
131 despite the regions having very different functions (Figure 1C). Indeed, the correlation between the similarity
132 profiles of the precentral gyrus and cuneus is $r = 0.975$. The similarity profile of human cerebellar crus 1
133 highlights another example of this homogeneity. The profile of crus 1 is similar to that of all regions of the
134 mouse cerebellum, with an average correlation of $r = 0.213$ and a standard deviation of $\sigma = 0.034$. Across
135 all regions, the variance of the correlations across cortical regions is $\sigma^2 = 0.0067$ while that across cerebellar
136 hemispheric regions is $\sigma^2 = 0.0013$, compared with a total variation of $\sigma^2 = 0.031$ across all entries in the
137 matrix.

138 So, although there is some distinguishing power in the profiles of regions at a finer scale, this is much smaller
139 than between coarse anatomical regions. This is also true for parts of the broad anatomical systems that are
140 part of the same functional system. This suggests that the regional expression patterns of mouse-human
141 homologous genes can be used to identify general similarities between the brains of the two species even
142 using a simple correlation measure, but the ability to identify finer scale matches might require a more
143 subtle approach.

144 **A latent gene expression space improves the resolution of mouse-human associations**
145

146 In the previous analyses, we showed that the expression profiles of homologous genes capture broad simi-
147 larities across the mouse and the human for the major subdivisions of the brain. Some information at a
148 finer resolution (e.g. within the isocortex) was also evident, but much less distinctive. Our next goal was
149 to investigate whether it is possible to leverage the gene expression data sets to relate mouse and human
150 brains to one another at a finer regional level. In order to do so, we sought to maximise the informational
151 value in the set of 2835 homologous genes by creating a new latent common space that exploits the regional

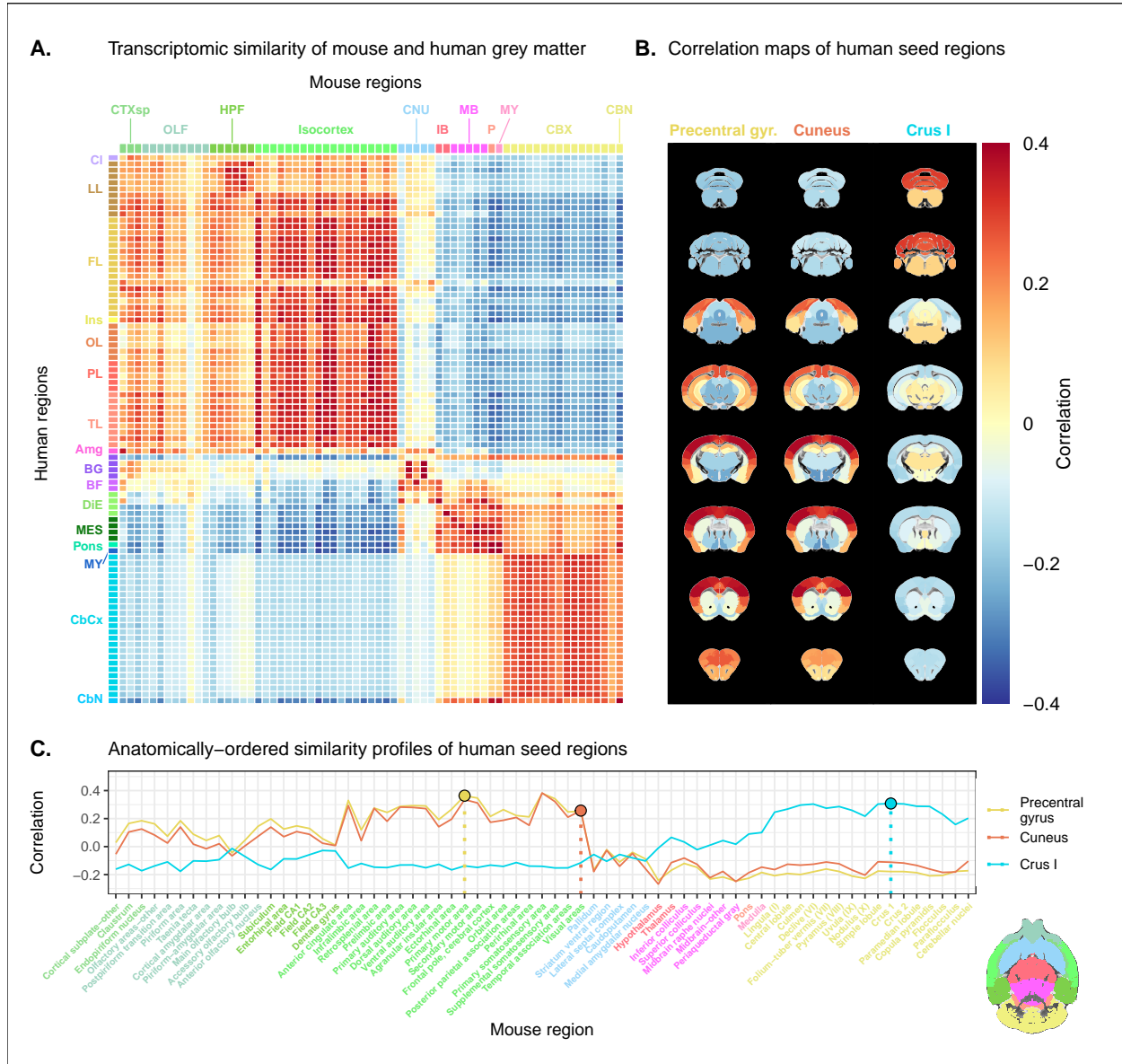


Figure 1. Transcriptomic similarity in the mouse and human brains. **(A)** Similarity matrix displaying the correlation between 67 mouse regions and 88 human regions based on the expression of 2835 homologous genes. Columns are annotated with 11 broad mouse regions: Cortical subplate (CTXsp), olfactory areas (OLF), hippocampal formation (HPF), isocortex, cerebral nuclei (CNU), interbrain (IB), midbrain (MB), pons (P), medulla (MY), cerebellar cortex (CBX), cerebellar nuclei (CBN). Rows are annotated with 16 broad human regions: Claustrum (Cl), limbic lobe (LL), frontal lobe (FL), insula (Ins), occipital lobe (OL), parietal lobe (PL), temporal lobe (TL), amygdala (Amg), basal ganglia (BG), basal forebrain (BF), diencephalon (DIE), mesencephalon (MES), pons, myelencephalon (MY), cerebellar cortex (CbCx), cerebellar nuclei (CbN). Broad patterns of similarity are evident between coarsely defined brain regions, while correlation patterns are mostly homogeneous within these regions. **(B)** Mouse brain coronal slices showing similarity profiles for the human precentral gyrus, cuneus and crus I. Correlation patterns for the precentral gyrus and cuneus are highly similar to one another and broadly similar to most isocortical regions. The crus I is homogeneously similar to the mouse cerebellum. **(C)** Anatomically-ordered line charts displaying the similarity profiles for the seed regions in (B). Dashed vertical lines indicate the canonical mouse homologue for each human seed. Annotation colours correspond to atlas colours from the AMBA and AHBA for mouse and human regions respectively. Source data 1. Related to Figure 1A, B, and C.

152 distinctiveness of the expression profiles.

153 The approach used in the previous analysis relied on using homologous genes as a common space between
154 the mouse and human brain. This approach effectively assigns equal value to each gene, whereas a more
155 powerful approach would be to weight genes by their ability to distinguish between different brain regions.
156 We investigated whether we could accomplish this by constructing a new set of variables from combinations
157 of the homologous genes. Our primary goal here was to transform the initial gene space into a new common
158 space that would improve the locality of the matches. However while we sought a transformation that would
159 allow us to recapitulate known mouse-human neuroanatomical homologues, we also wanted to avoid directly
160 encoding such correspondences in the transformation. Using this information as part of the optimization
161 process for the transformation would run the risk of driving the transformation towards mouse-human pairs
162 that are already known. While we are interested in being able to recover such matches, we are equally
163 interested in identifying novel and unexpected associations between neuroanatomical regions in the mouse
164 and human brains (e.g. one-to-many correspondences). Given these criteria, our approach to identifying an
165 appropriate transformation was to train a multi-layer perceptron classifier on the data from the AMBA. The
166 classifier was tasked with predicting the 67 labels in our mouse atlas from the voxel-wise expression of the
167 homologous genes (Figure 2A).

168 While the model could have been trained using the data from either species, we chose to use the mouse
169 data because it provides continuous coverage of the entire brain and is thus better suited to this purpose.
170 In training the model to perform this classification task, we effectively optimize the network architecture
171 to identify a transformation from the input gene space to a space that encodes information about the
172 delineation between mouse brain regions. To extract this transformation, we removed the output layer from
173 the trained neural network. The resulting architecture defines a transformation from the input space to
174 a lower-dimensional gene expression latent space. We then applied this transformation to the mouse and
175 human gene-by-region expression matrices to obtain representations of the data in the latent common space
176 (Figure 2B). Finally, we used these gene expression latent common space matrices to compute the new
177 similarity matrix (Figure 2C). Since the optimization algorithm used to train the perceptron features an
178 inherent degree of stochasticity, we repeated this training and transformation process 500 times to generate
179 a distribution of latent spaces and similarity matrices over training runs. Although the neural network and
180 associated latent space do not directly provide information about which genes are most important for the
181 classification of specific mouse atlas labels, this type of information can be derived from the model using
182 attribution methods such as integrated gradients (Figure 2-figure supplement 1) (Sundararajan et al., 2017).
183 Each brain region in the classification task is associated with the input genes in different ways, such that

184 there isn't a single weighting of gene importance for the entire model. While most genes contribute to the
 185 classification of any given label in some capacity, it is often the case that the network relies on a reduced
 186 subset of genes to arrive at a decision. For example, the genes *Prrg2* and *Cd4* were found to be most
 187 influential for the classification of the caudoputamen, when the feature attributions were averaged over all
 188 training runs. In contrast, *Rfx4* and *Ghra3* were the most influential for the classification of the primary
 189 motor area. In some cases, the spatial expression pattern of the gene clearly shows a demarcation of the
 190 region of interest (e.g. *Cd4*), but this is not always the case, nor is it necessary, as the network learns from
 191 the entire gene expression signature of all voxels.

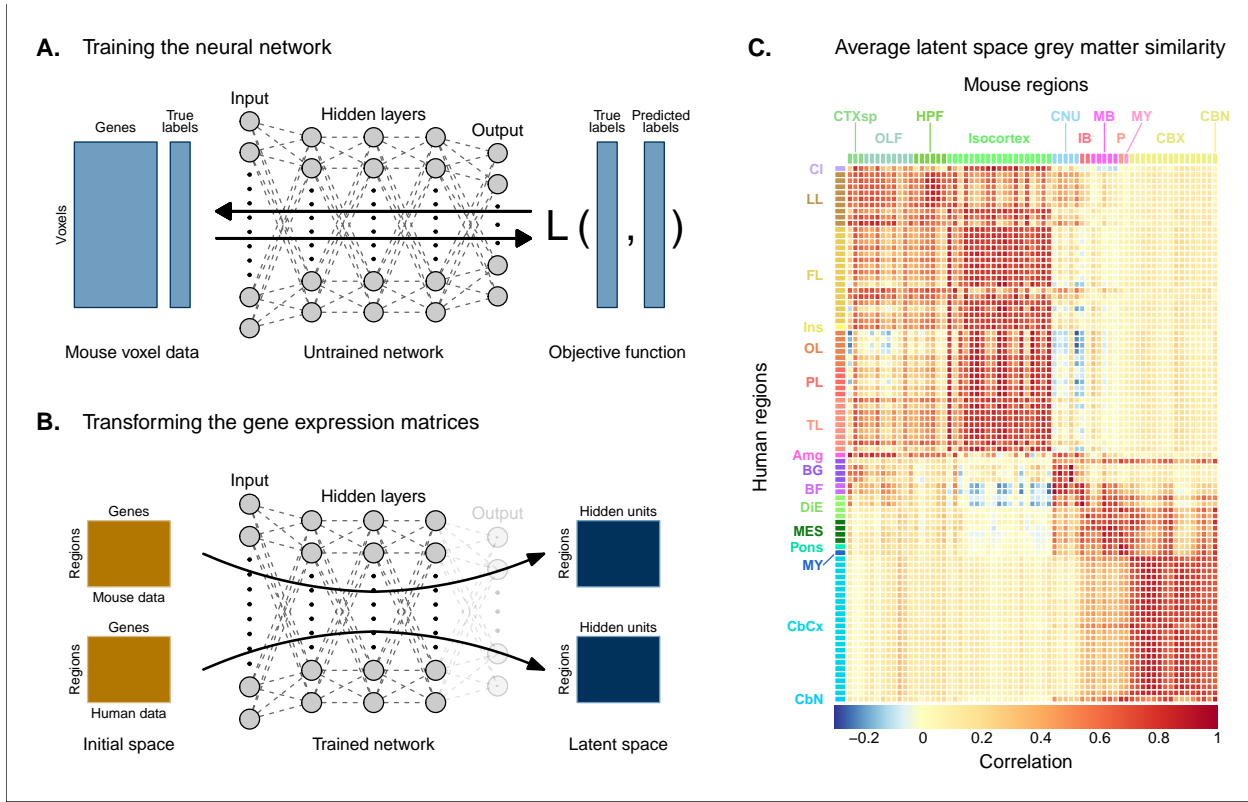


Figure 2. Creating a new common space. **(A)** Voxel-wise expression maps from 2835 homologous genes in the AMBA were used to train the neural network to classify each mouse voxel into one of 67 atlas regions. **(B)** Once the network is trained, the output layer is removed. The mouse and human regional gene expression matrices are passed through the network, resulting in lower-dimensional latent space representations of the data. The training and transformation process was repeated 500 times. **(C)** A similarity matrix displaying the gene expression latent space correlation between mouse and human regions, averaged over 500 neural network training runs. Similar brain regions exhibit very high correlation values. Column and row annotations as described in Figure 1. Source data 1. Related to Figure 2C. Source data 2. Related to Figure 2C. Source data 3. Related to Figure 2C. Figure supplement 1. Multi-layer perceptron feature importance for the classification of the caudoputamen, the primary motor area, and the infralimbic area.

192 To assess whether the latent space representations of the data improved the resolution of the mouse-human
 193 matches, we considered two criteria. The first was whether the similarity profiles of the mouse atlas regions
 194 were more localized within the corresponding broad regions of interest (e.g. primary motor area within
 195 isocortex), compared with their similarity profiles in the original gene space. We term this the locality
 196 criterion. The second criterion was whether the degree of similarity between canonical neuroanatomical

homologues improved in this new latent common space. We term this the homology criterion. The locality criterion tells us about our ability to extract finer-scale signal in these profiles, while the homology criterion informs us about our ability to recover expected matches in this finer-scale signal. To evaluate these criteria, we computed ranked similarity profiles for every region in the mouse brain, ordered such that a rank of 1 indicates the most similar human region. In addition, given the difference in absolute value between the input gene space and gene expression latent space correlations, we scaled the similarity profiles to the interval $[0, 1]$ in order to make comparisons between the spaces.

We evaluated the locality criterion by examining the decay rate of the top of the similarity profiles. We reasoned that the plateau of similarity to a broad brain region, as seen in the anatomically-ordered similarity matrices and profiles (Figure 1, A and C; Figure 2C), would correspond to a similar plateau at the head of the rank-ordered profiles. Moreover, the emergence of local signal would manifest as an increase in the range between the peaks and troughs within the broad region. In the rank-ordered profiles, this would correspond to a faster rate of decay at the head of the profile. In order to quantify this decay, we computed the rank at which each region's similarity profile decreased to a scaled value of 0.75. This was calculated for every mouse region in the initial gene space, as well as in each of the 500 gene expression latent spaces. As a measurement of performance between the two representations of the data, we then took the difference in this rank between each of the latent spaces and the original gene space (Figure 3A). A negative rank difference indicates an improvement in the latent space.

Examining the structure-wise distributions of these rank differences, we found that for the majority of regions in our mouse atlas, the classification approach resulted in either an improvement in the amount of locality within a broad region, or no difference from the original gene space (Figure 3, B and C). We quantified the improvement overall by fitting a logistic regression model with no predictors to the mean rank differences of each of the atlas regions. We considered the success condition for the Bernoulli trials to be a mean rank difference less than or equal to zero. The model estimate for the Bernoulli probability – which we denote p_B to distinguish from the p-value p – was $p_B = 0.78$ with a 95% confidence interval of $[0.66, 0.86]$. In other words, 52 of the 67 brain regions saw an improvement on average when using the latent spaces. The probability of obtaining at least as many successes as this under the null model, i.e. a binomial distribution with $p_B = 0.50$ and $n = 67$, is $p = 8.64 \cdot 10^{-7}$. We additionally evaluated the same kind of logistic regression on a region-wise basis to quantify how often the latent spaces resulted in an improvement for individual brain regions (Figure 3C). We found that for 46 regions (69%), the model estimated the probability to be at least as high as $p_B = 0.95$. While confidence intervals varied around this estimate, the range between the upper and lower bound was only ever as high as 0.04. For 53 of the 67 regions (79%), the q-values,

229 i.e. p-values adjusted for multiple comparisons, were effectively null, with the largest being $q = 3.77 \cdot 10^{-16}$.
230 Of the remaining 14 regions, 13 had q-values equal to 1 and one region, the periacqueductal gray, had a
231 q-value of $q = 0.854$. The regions with the smallest estimates for the Bernouilli probabilities are the dentate
232 gyrus ($p_B = 0.0$, no variance, $q = 1$), the striatum ventral region ($p_B = 0.016$, 95% CI [0.008, 0.032], $q = 1$),
233 and the lateral septal complex ($p = 0.016$, 95% CI [0.008, 0.032], $q = 1$). The remaining regions with
234 $q = 1$ are all subcortical and fall under the broad subdivisions of cerebral nuclei, olfactory areas, interbrain,
235 midbrain, pons, medulla, and cerebellar nuclei. Beyond this binary measure of improvement, some regions
236 exhibited a large range of differences in rank over the various latent spaces. In particular regions like the
237 main olfactory bulb (mean rank difference of $\mu = 10$, 95% CI [-12, 33]) and accessory olfactory bulb $\mu = 9$,
238 95% CI [-13, 31]) exhibit a substantial degree of variance. Other than these two areas, regions within
239 the olfactory areas (e.g. piriform area) were among those that benefited the most from the classification
240 approach, showing improvement in all sampled latent spaces, with all Bernouilli probability estimates equal
241 to 1 and all q-values equal to 0. While the effects, i.e. rank differences, are smaller, the similarity profiles of
242 regions belonging to the isocortex and cerebellar cortex also saw an improvement in locality. All models for
243 isocortical areas returned Bernouilli probability estimates greater than $p_B = 0.85$ and q-values that were at
244 most $q = 1.35 \cdot 10^{-67}$. Moreover, 9 of the 19 isocortical regions were improved in all latent spaces, i.e. $p_B = 1$.
245 Brain regions belonging to the cerebellar cortex saw similar improvement. In contrast, regions belonging to
246 the cerebral nuclei, the diencephalon, midbrain and hindbrain did not see much improvement in this new
247 common space, with an average Bernouilli probability estimate of $p_B = 0.36$ for this subset. Other than the
248 caudoputamen ($p_B = 0.99$, 95% CI [0.97, 1.00], $q = 1.35 \cdot 10^{-139}$), the superior colliculus ($p_B = 0.90$, 95% CI
249 [0.87, 0.92], $q = 9.82 \cdot 10^{-81}$), and the inferior colliculus ($p_B = 0.75$, 95% CI [0.71, 0.78], $q = 3.12 \cdot 10^{-30}$),
250 all regions in this subset return q-values equal to 1. For many such regions the degree of locality appears
251 to be worse in this space, though only by a small number of ranks, e.g. striatum ventral region (mean rank
252 difference of $\mu = 4$, 95% CI [1, 7]) and lateral septal complex ($\mu = 6$, 95% CI [0, 11]). Indeed, computing
253 the average rank difference over this subset of regions across all latent spaces, we find $\mu = 2$ with 95%
254 confidence interval [-5, 8]. These results demonstrate that the supervised learning approach used here can
255 improve the resolution of neuroanatomical correspondences between the mouse and human brains, though
256 the amount of improvement varies over the brain. Regions that were already well-characterized using the
257 initial set of homologous genes (e.g. subcortical regions) did not benefit tremendously, but numerous regions
258 in the cortical plate and subplate, as well as the cerebellum, saw an improvement in locality in this new
259 common space.

260 While the supervised learning approach improved our ability to identify matches on a finer scale for a number

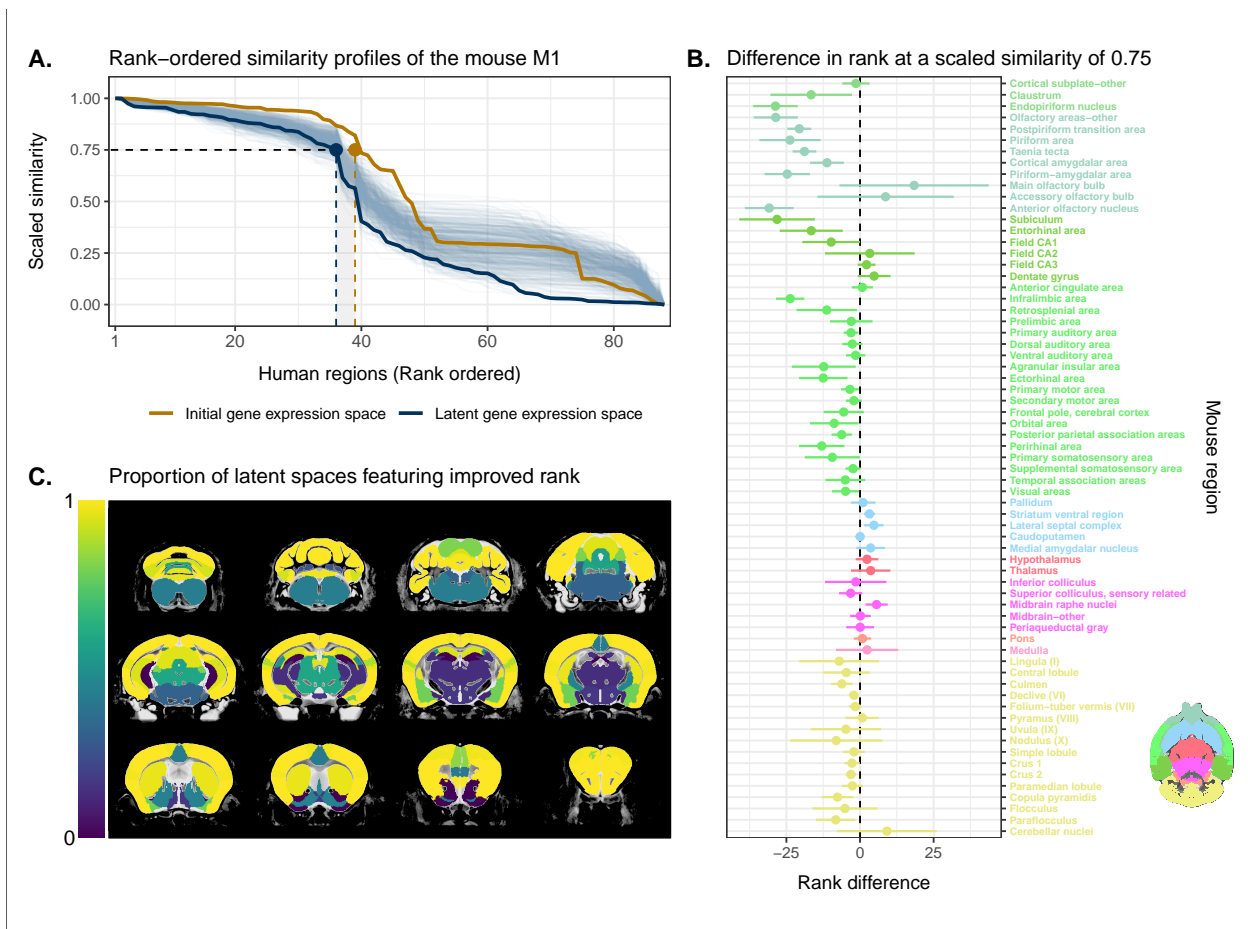


Figure 3. Quantifying improvement in locality in gene expression latent space. **(A)** The amount of local signal within a broadly similar region of the brain for a finer seed region's (e.g. primary motor area) similarity profile can be quantified by the decay rate of the head of the rank-ordered profile. Decay rate was quantified by computing the rank at a similarity of 0.75. This metric was compared between the initial gene expression space (orange line) and every gene expression latent space resulting from repeated training of the neural network (every blue line is a training outcome, heavy blue line serves as an example). A negative difference between these rank metrics indicates an improvement in locality in the latent space. **(B)** Structure-wise distributions of differences in rank at a similarity of 0.75 between the initial gene expression space and the gene expression latent spaces. Points and error bars represent mean and 95% confidence interval. Dashed black line at 0 indicates the threshold for improvement in one space over the other. Colours correspond to AMBA annotations as in Figures 1 and 2. Binomial likelihood (logistic regression) estimate of $p_B = 0.78$ with %95 CI [0.66, 0.86]. The probability of obtaining at least this many successes under the null binomial distribution, $B(67, 0.5)$, is $p = 8.64 \cdot 10^{-7}$. **(C)** Proportion of perceptron training runs resulting in an improvement or null difference in the gene expression latent space compared with the initial space, estimated using region-wise logistic regressions. Cortical and cerebellar regions exhibit high proportions of improvement, while subcortical regions are less likely to be improved by the classification process. Source data 1. Related to Figure 3A. Source data 2. Related to Figure 3B. Source data 3. Related to Figure 3C.

of brain regions, this does not necessarily mean that those improved matches are biologically meaningful. The second criterion for evaluating the performance of the neural network addresses whether this improvement in locality captures what we would expect in terms of known mouse-human homologies. To this end, we examined the degree of similarity between established mouse-human neuroanatomical pairs, both in the initial gene expression space and in the set of latent spaces. We began by establishing a list of 36 canonical mouse-human homologous pairs on the basis of common neuroanatomical labels in our atlases. For each of these regions in the mouse brain, we compared the rank of the canonical human match in the rank-ordered similarity profiles between the latent spaces and the original gene expression space (Figure 4A). The lower the rank, the more similar the canonical pair, with a rank of 1 indicating maximal similarity. As described above, we evaluated the overall performance of the classification approach by running a logistic regression using the average latent space rank difference over all regions in our subset. Here we find an estimated Bernouilli probability of $p_B = 0.64$ with 95% confidence interval [0.47, 0.78]. Under the null binomial distribution, $B(36, 0.5)$, the probability of getting at least as many successes as this is $p = 0.033$. We also evaluated the model for each brain region and found that 30 of the 36 regions (83%) return Bernouilli probability estimates of at least $p_B = 0.80$. Under the null binomial distribution, $B(500, 0.5)$, we find that the largest q-value among these 30 regions is $q = 4.39 \cdot 10^{-54}$. Moreover, 24 regions (67%) return Bernouilli probability estimates of at least $p_B = 0.90$ and 8 regions show improvement in all latent spaces, i.e. $p_B = 1$ and $q = 0$ (Figure 4B). Among these 8 regions are the claustrum, the piriform area, the primary motor and somatosensory areas, and the crus 2. Additional examples of the many regions that demonstrate improvement include: the primary auditory area ($p_B = 0.83$, 95% CI [0.80, 0.86], $q = 1.80 \cdot 10^{-55}$), the pallidum ($p_B = 0.86$, 95% CI [0.83, 0.89], $q = 3.63 \cdot 10^{-65}$), and the crus 1 ($p_B = 0.92$, 95% CI [0.90, 0.94], $q = 7.68 \cdot 10^{-95}$). Once again we find that many regions in the sub-cortex do not benefit greatly from the gene expression latent spaces, since the initial gene set was already recapitulating the appropriate match with maximal similarity. We find that the striatum ventral region, caudoputamen, hypothalamus, and pons are maximally similar to their canonical matches in at least 95% of latent spaces. In such cases, the classification approach performs as well as the original approach. While these probability estimates provide a sense of how often an improvement is returned, it is important to note that many regions in this set exhibit a substantial degree of variance over the latent spaces in the ranking of the canonical pairs, e.g. the primary auditory area ($\mu = 9$, 95% CI [1, 19]), the visual areas ($\mu = 18$, 95% CI [7, 29]), the paraflocculus ($\mu = 16$, 95% CI [2, 29]). This is especially apparent for cerebellar regions, indicating some instability in the neural network's ability to recover these matches.

Together, these results demonstrate that the multi-layer perceptron classification approach improves our abil-

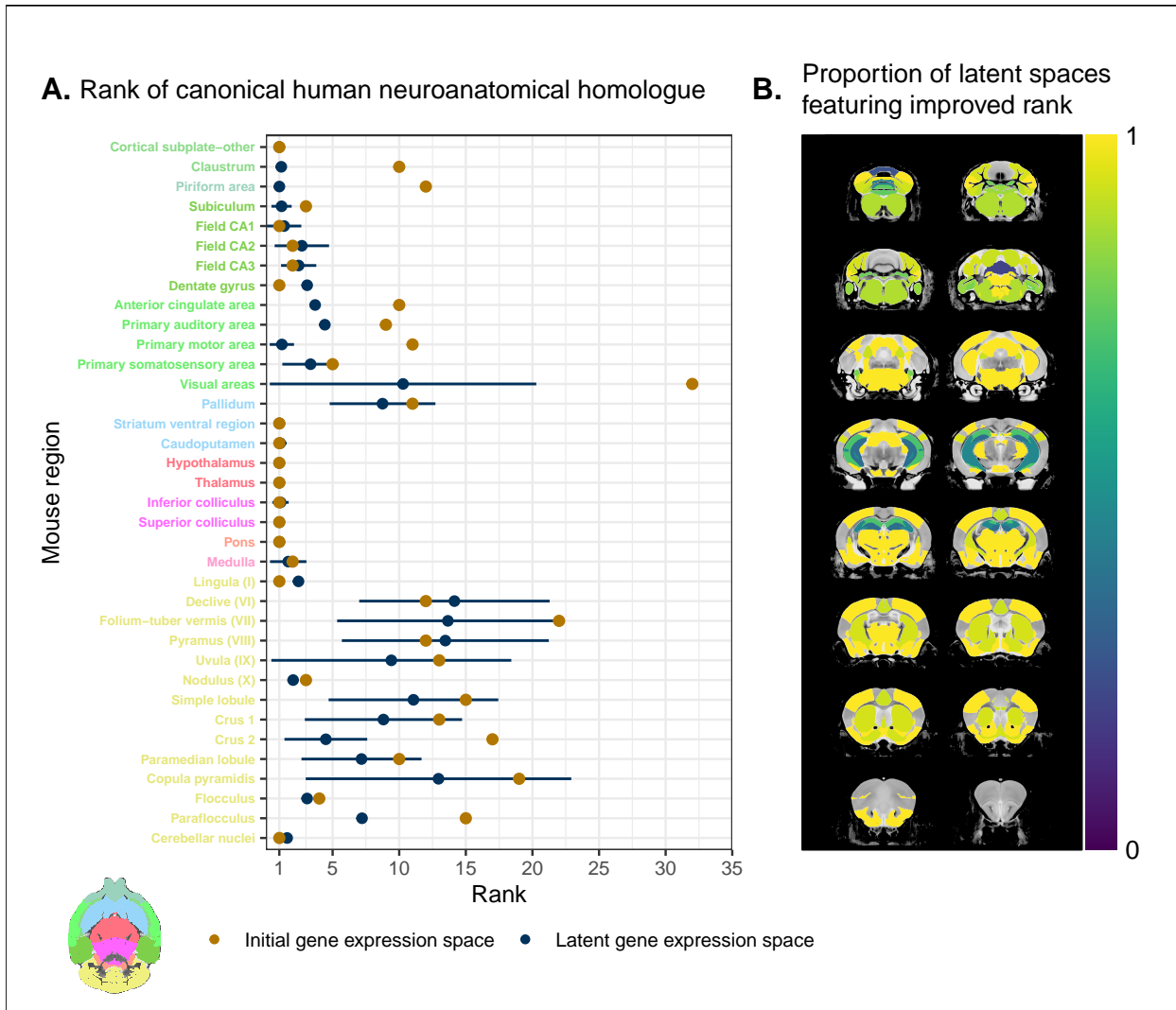


Figure 4. Recovering canonical neuroanatomical pairs in gene expression space. **(A)** Comparison between the ranks of canonical human matches for mouse seed regions between the initial gene expression space and gene expression latent spaces. Points and error bars represent mean and 95% confidence interval. Intervals are truncated at a minimal rank of 1, since values below this are meaningless. Mouse region names are coloured according to the AMBA palette. Binomial likelihood estimate of $p = 0.64$ with 95% CI [0.47, 0.78]. The probability of obtaining at least this many successes under the null binomial distribution, $B(36, 0.5)$, is $p = 0.033$. **(B)** Proportion of latent spaces resulting in an improvement or null difference compared with the initial gene space, estimated using region-wise logistic regressions. Uncoloured voxels correspond to regions with no established canonical human match. Source data 1. Related to Figure 4A. Source data 2. Related to Figure 4B.

293 ity to resolve finer scale mouse-human neuroanatomical matches within the broadly similar regions obtained
294 using the initial gene expression space. By training a classifier to predict the atlas labels in one species, we
295 were able to generate a new common space that amplified the amount of local signal within broadly similar
296 regions while also improving our ability to recover known mouse-human neuroanatomical pairs.

297 **Cortical areas involved in sensorimotor processing show greater transcriptomic
298 similarity than supramodal areas**

299 It is well established that the brains of most, if not all, extant mammalian species follow a common organi-
300 zational blueprint inherited from an early mammalian ancestor (Kaas, 2011a). A number of cortical subdivi-
301 sions have consistently been identified in members of many distantly related mammalian species (Krubitzer,
302 2007) and hypothesized to have been present in the common ancestor of all mammals (Kaas, 2011a). While
303 it is clear that basic sensorimotor cortical regions are found in the majority of mammals, including mice and
304 humans, there is much debate about the extent to which cortical areas involved in supramodal processing
305 are conserved across mammalian taxa. Although some supramodal regions were likely present in the earliest
306 mammals, including some cingulate regions and an orbitofrontal cortex (Kaas, 2011a), since the divergence
307 of mouse and human lineages some 80 million years ago, the primate neocortex has undergone substantial
308 expansion and re-organization (Kaas, 2012). Indeed, when comparing the human neocortex even to primate
309 model species, this is the likely locus of areas that cannot be easily translated between species (Rogier B.
310 Mars et al., 2018b). As a result, it is important to investigate whether our between-species mapping is more
311 successful in somatosensory areas than supramodal areas.

312 We assessed the similarity between mouse and human isocortical areas using the pairwise correlations in each
313 of the gene expression latent spaces returned from the multi-layer perceptron. For every region in the mouse
314 isocortex, we evaluated the distribution of maximal correlation values over latent spaces (Figure 5A). While
315 the region-wise variance for each isocortical area was large, we found that, on average, sensorimotor regions
316 exhibited higher maximal correlation values than supramodal regions (linear regression with binary predictor:
317 $\beta = -0.042$, 95% CI $[-0.087, 0.003]$, $t(17) = -1.854$, $p = 0.0812$). The mouse primary somatosensory
318 ($r = 0.96$, 95% CI $[0.93, 0.98]$) and motor ($r = 0.95$ with 95% CI $[0.92, 0.98]$) areas have the highest average
319 maximal correlation values. We additionally examined the distributions of maximal correlation, grouped by
320 cortex type (Figure 5B). To generate these distributions, we computed average maximal correlation values
321 by cortex type in each of the latent spaces. Here too we find that that sensorimotor regions are associated
322 with higher maximal correlation values on average compared with supramodal areas (linear mixed-effects

323 regression: $\beta = -0.042$, 95% CI $[-0.044, -0.040]$, $t(499) = -49.9$, $p < 2 \cdot 10^{-16}$). These distributions
324 demonstrate that sensorimotor isocortical regions exhibit more similarity overall on the basis of homologous
325 gene expression than do supramodal regions.

326 While we found that sensorimotor isocortical areas in the mouse brain were more similar to human brain
327 regions than supramodal areas, the distributions of maximal correlation do not speak to the neuroanatomical
328 patterns of organization for these matches. To understand how the similarity patterns of mouse and human
329 cortical subdivisions were organized, we used hierarchical clustering to cluster mouse and human isocortical
330 regions on the basis of their similarity profiles in the average gene expression latent space (Figure 5C). This
331 allows us to examine the similarity of regions to one another within and across brains at multiple levels
332 simultaneously.

333 At a high level, we find a striking segregation of the mouse isocortex into one main cluster that corresponds
334 to regions that are primarily engaged in sensorimotor processing and separate clusters of regions that are
335 supramodal. All of the sensorimotor areas cluster together, but two supramodal areas also form part of this
336 cluster: the posterior parietal association areas and the anterior cingulate cortex. The mouse sensorimotor
337 cluster is characterized by high correlation values to human sensorimotor regions like the precentral gyrus, the
338 cuneus, and the postcentral gyrus, as well as low correlation values to the piriform cortex and paraterminal
339 gyrus. At this level of clustering, the remaining mouse supramodal subdivisions form three clusters. The
340 retrosplenial area belongs to its own cluster, while the infralimbic and perirhinal areas cluster together.
341 The similarity profile of the retrosplenial area is most similar to the sensorimotor cluster, and these two
342 clusters are combined in the three-cluster solution. The remaining two mouse clusters are characterized by
343 low correlations to the human cluster containing sensorimotor areas. This is especially true for the cluster
344 containing the infralimbic and perirhinal areas.

345 On the human side, the four-cluster solution also features a sensorimotor cluster, which contains regions
346 like the pre- and post-central gyri, the cuneus, and Heschl's gyrus. This cluster exhibits a high degree
347 of similarity to the mouse sensorimotor cluster and low similarity to the mouse supramodal clusters. The
348 isocortical regions not belonging to this cluster are split into three clusters. The majority of these remaining
349 regions form a large cluster that contains areas like the cingulate gyrus and the frontal pole. The parolfactory
350 gyri, parahippocampal gyrus and temporal pole form a separate cluster that exhibits high correlation to the
351 mouse entorhinal, orbital, and prelimbic areas. Finally, the paraterminal gyrus and piriform cortex are
352 clustered together and exhibit high similarity to the mouse infralimbic area and low similarity to the mouse
353 sensorimotor cluster.

354 We additionally ran hierarchical clustering on the isocortical similarity matrix in the original homologous

355 gene space. While the cluster annotations were not substantially different in this space, we observed that
356 the Euclidean distances within and between clusters were smaller compared with the latent space clustering,
357 further confirming that the perceptron classification approach improves the segregation of brain regions in
358 the gene expression common space (Figure 5D).

359 Overall, we observe a greater degree of similarity between mouse and human cortical regions involved in
360 basic sensorimotor processing compared with supramodal or association areas. This is in line with the large
361 body of existing research that suggests that sensory and motor areas of the isocortex are conserved across
362 the brains of mammals. While sensorimotor areas exhibit a greater degree of similarity than supramodal
363 areas, the neuroanatomical pattern of correspondences obtained using mouse-human homologous genes is
364 not at the level of individual cortical areas. Still, using a clustering approach we identified clear distinctions
365 in the patterns of similarity between sensorimotor and supramodal areas, especially for regions in the mouse
366 isocortex.

367 Transcriptomic comparison of the mouse and human striatum

368 We have focused here on comparing mouse and human brain organization using transcriptomic data, with
369 a latent space based on homologous genes as the common space between the two species. To date, common
370 space comparisons between the mouse and human brain have only been performed using functional con-
371 nectivity (Balsters et al., 2020; Schaeffer et al., 2020). As a case in point, Balsters et al. (2020) compared
372 mouse and human striatal organization using this measure. They found that the nucleus accumbens was
373 highly conserved between mice and humans, and that voxels in the posterior part of the human putamen
374 were significantly similar to the lateral portion of their mouse caudoputamen parcellation. Additionally,
375 they report that 85% of voxels in the human striatum were not significantly similar to any of their mouse
376 striatal seeds, and that 25% of human striatal voxels were significantly dissimilar compared with the mouse.
377 These differences were understandable, as they involved parts of the human striatum that connected to parts
378 of prefrontal cortex that have no known homolog in the mouse (Neubert et al., 2014). However, it is not
379 necessarily the case that between-species differences in connectivity are associated with distinct architectonic
380 or molecular signatures. Therefore, we investigated the patterns of similarity between the mouse and human
381 striata on the basis of gene expression using the neural network latent space representations.

382 We first identified the striatal regions present in the Allen human dataset: the caudate, the putamen, and the
383 nucleus accumbens. We evaluated the correlation between the microarray samples in these regions and every
384 region in the mouse atlas. Based on these correlation values, we focused our analysis on the four mouse

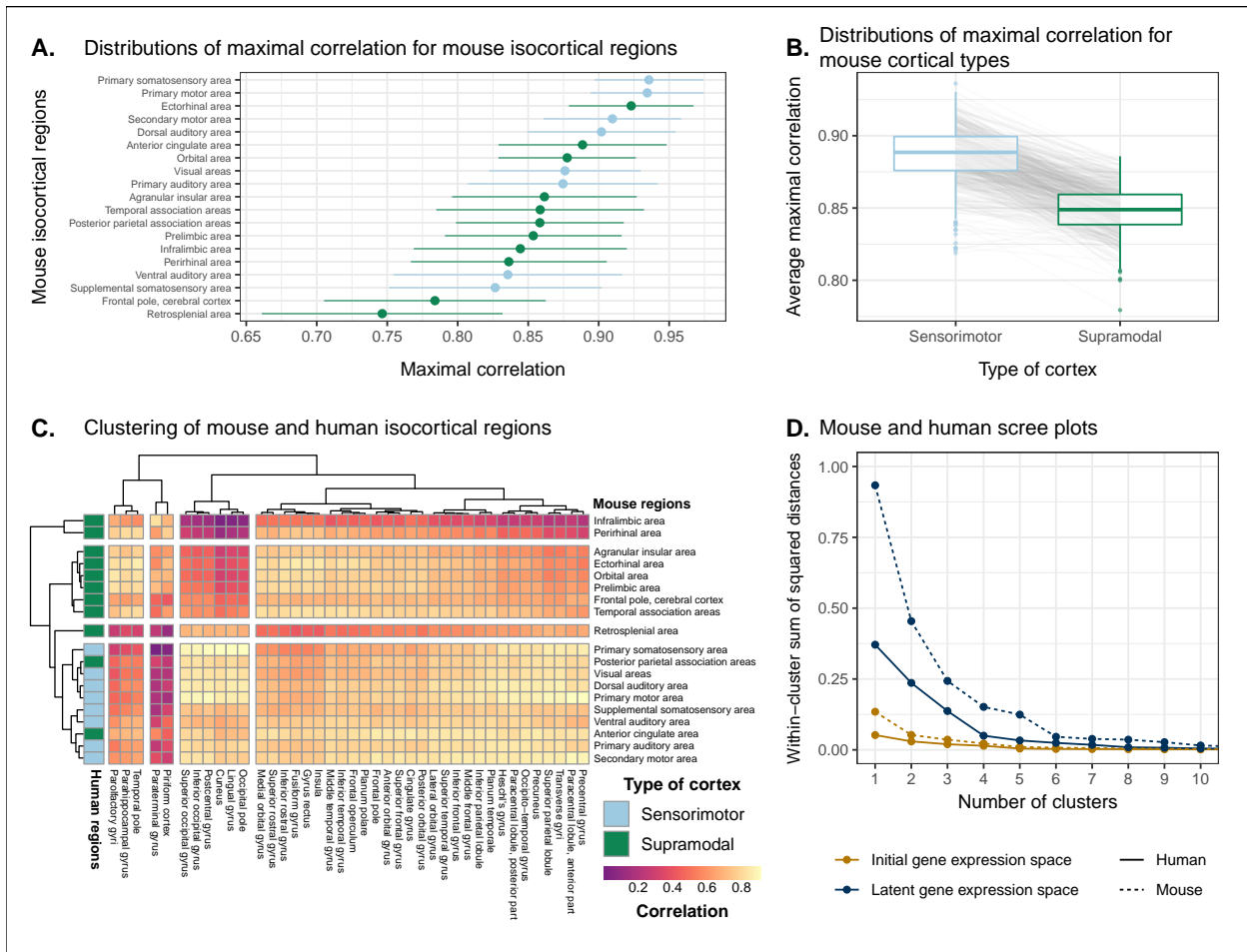


Figure 5. Similarity of mouse-human isocortical regions. **(A)** Maximal correlation distributions of mouse isocortical regions. Points and error bars represent mean and 95% confidence interval over latent space samples. Linear regression using average maximal correlation values: $\beta = -0.042$, 95% CI $[-0.087, 0.003]$, $t(17) = -1.854$, $p = 0.0812$. **(B)** Distributions of average maximal correlation for sensorimotor and supramodal isocortical areas in each gene expression latent space. Grey lines correspond to individual latent spaces. Linear mixed-effects regression: $\beta = -0.042$, 95% CI $[-0.044, -0.040]$, $t(499) = -49.9$, $p < 2 \cdot 10^{-16}$. **(C)** Hierarchical clustering of mouse and human isocortical regions based on average latent space correlation values. Mouse regions are annotated as sensorimotor or supramodal. Four clusters were chosen for visualization using the elbow method. **(D)** Within-cluster sum of squared distances for different numbers of mouse and human isocortical clusters in the average latent space and initial homologous gene space. Source data 1. Related to Figure 5A and B. Source data 2. Related to Figure 5C. Source data 3. Related to Figure 5D.

385 regions that were consistently the most similar across all latent spaces: the caudoputamen, the nucleus
386 accumbens, the fundus of striatum, and the olfactory tubercle. For each of the human striatal regions, we
387 then calculated the average correlation over the samples to each of the mouse targets. We examined the
388 distribution of these average correlation values over the latent spaces (Figure 6A). We find that the human
389 caudate and putamen consistently exhibit the strongest degree of similarity to the mouse caudoputamen.
390 The median of the distributions for the caudate-caudoputamen pairs and putamen-caudoputamen pairs is
391 0.93, with modal values of 0.92 and 0.94, respectively. All latent spaces return correlations greater than
392 0.85 for caudate-caudoputamen and putamen-caudoputamen pairs. Beyond this expected top match, the
393 caudate and putamen both exhibit high similarity to the nucleus accumbens and the fundus of striatum,
394 with median correlation values of about 0.80. Neither of these target regions is consistently more similar to
395 the mouse caudoputamen over all latent spaces.

396 While the similarity of the caudate and the putamen to the caudoputamen is unsurprising, the story is
397 not as clear for the human nucleus accumbens. We find that the variance in correlation calculated over all
398 mouse targets is lower ($\sigma = 0.04$) compared with the equivalent variances for the caudate ($\sigma = 0.08$) and
399 putamen ($\sigma = 0.08$), indicating less specificity to any one mouse striatal target. In particular, the human
400 nucleus accumbens isn't as specifically similar to the mouse nucleus accumbens in the way that the caudate
401 and putamen are similar to the caudoputamen. The mouse target distributions are right-shifted compared
402 with those for the caudate and putamen, with median values of 0.89, 0.86, and 0.87 for the mouse nucleus
403 accumbens, caudoputamen, and fundus of striatum, respectively. The human accumbens also exhibits a high
404 degree of similarity to the mouse olfactory tubercle, the distribution of which is also right-shifted compared
405 with the caudate and putamen.

406 Given the high correlation of the human caudate and putamen to the mouse caudoputamen, as well as the
407 finding reported by Balsters et al. about the similarity of the lateral caudoputamen to the putamen, we were
408 curious as to whether we could identify sub-regional patterns of similarity in the caudoputamen and other
409 striatal regions using these gene expression data. To probe this question, we first examined the average
410 latent space correlation between each voxel in the mouse striatum and every region in the human atlas. We
411 created brain maps for the human regions that exhibited the highest mean correlation values, averaged over
412 mouse striatal voxels: the caudate, the putamen, the nucleus accumbens, and the septal nuclei (Figure 6B).
413 We find that voxels in the caudoputamen exhibit a homogeneous pattern of similarity to both the caudate
414 and the putamen. On average, voxels in the caudoputamen have a correlation of 0.92 to the caudate and
415 0.91 to the putamen, with standard deviations of 0.05 and 0.06 respectively. The caudate and putamen are
416 associated with correlations of at least 0.90 in 79% and 73% of caudoputamen voxels. A number of voxels

417 are also highly similar to the human nucleus accumbens, with an average correlation value of 0.86 and 30%
418 of voxels returning a correlation of at least 0.90. The caudoputamen voxels most similar to the nucleus
419 accumbens lie in the ventral-rostral part of the region. Of course, voxels in the mouse nucleus accumbens are
420 also highly similar to the human nucleus accumbens, with an average of 0.89 and standard deviation of 0.06.
421 While the human nucleus accumbens is the most strongly correlated region, a number of voxels also exhibit
422 reasonably strong correlations to the substantia innominata and the amygdala. Indeed, 88% of voxels in the
423 accumbens are correlated at a value of 0.7 or higher to the amygdala, and 57% of voxels pass this threshold
424 for the substantia innominata.

425 We additionally examined the proportion of latent spaces in which each voxel in the mouse striatum was
426 maximally similar to the human target regions (Figure 6C). As expected, we find that voxels in the cau-
427 doputamen are most often maximally similar to the human caudate and putamen, with 77% of voxels in
428 the caudoputamen being maximally similar to the caudate or putamen in at least 95% of latent spaces, and
429 59% of voxels being maximally similar to one of those targets in all latent spaces. Interestingly, we observe
430 the emergence of a continuous bilateral pattern of specificity to the caudate and putamen, with voxels in the
431 rostral and lateral-caudal parts of the caudoputamen being maximally similar to the caudate in a high pro-
432 portion of latent spaces. In contrast, while voxels in the medial-rostral part of the caudoputamen are often
433 maximally similar to the caudate, they are also maximally similar to the putamen in some of latent spaces.
434 This map highlights subtle differences in the similarity between caudoputamen voxels and the caudate or
435 putamen. While this pattern distinguishes the two regions on the basis of which is the top match, individual
436 voxels have very similar correlation values to the targets (Figure 6B), with a mean difference in correlation
437 of only 0.01. Beyond the caudoputamen, we find that the accumbens and olfactory tubercle in the mouse
438 are consistently similar to the human nucleus accumbens, with 84% of mouse accumbens voxels and 75% of
439 olfactory tubercle voxels having the human accumbens as their top match in at least 80% of latent spaces.
440 For those voxels below this threshold, the human regions that are most often the top match are the amygdala
441 and the piriform cortex.

442 Overall, we observe a strong association between the mouse caudoputamen and both the human caudate and
443 putamen. While we find a subtle pattern of specificity to either region among voxels in the caudoputamen on
444 the basis of maximal similarity, the high degree of similarity in the correlation values to each region suggests
445 that the majority of voxels in the caudoputamen are equally similar to the caudate and the putamen on the
446 basis of the expression of mouse-human homologous genes. We also find that the nucleus accumbens is well
447 conserved across species. However the region also exhibits patterns of similarity that go beyond the simple
448 one-to-one match. The human accumbens features similar correlation values to the mouse caudoputamen

449 and fundus of striatum, in addition to the accumbens proper, with no sharp distinction between these regions.
 450 It also exhibits a larger degree of similarity to the mouse olfactory tubercle. This is also seen in the mouse
 451 striatum, where voxels in the accumbens and the olfactory tubercle map onto the human accumbens.

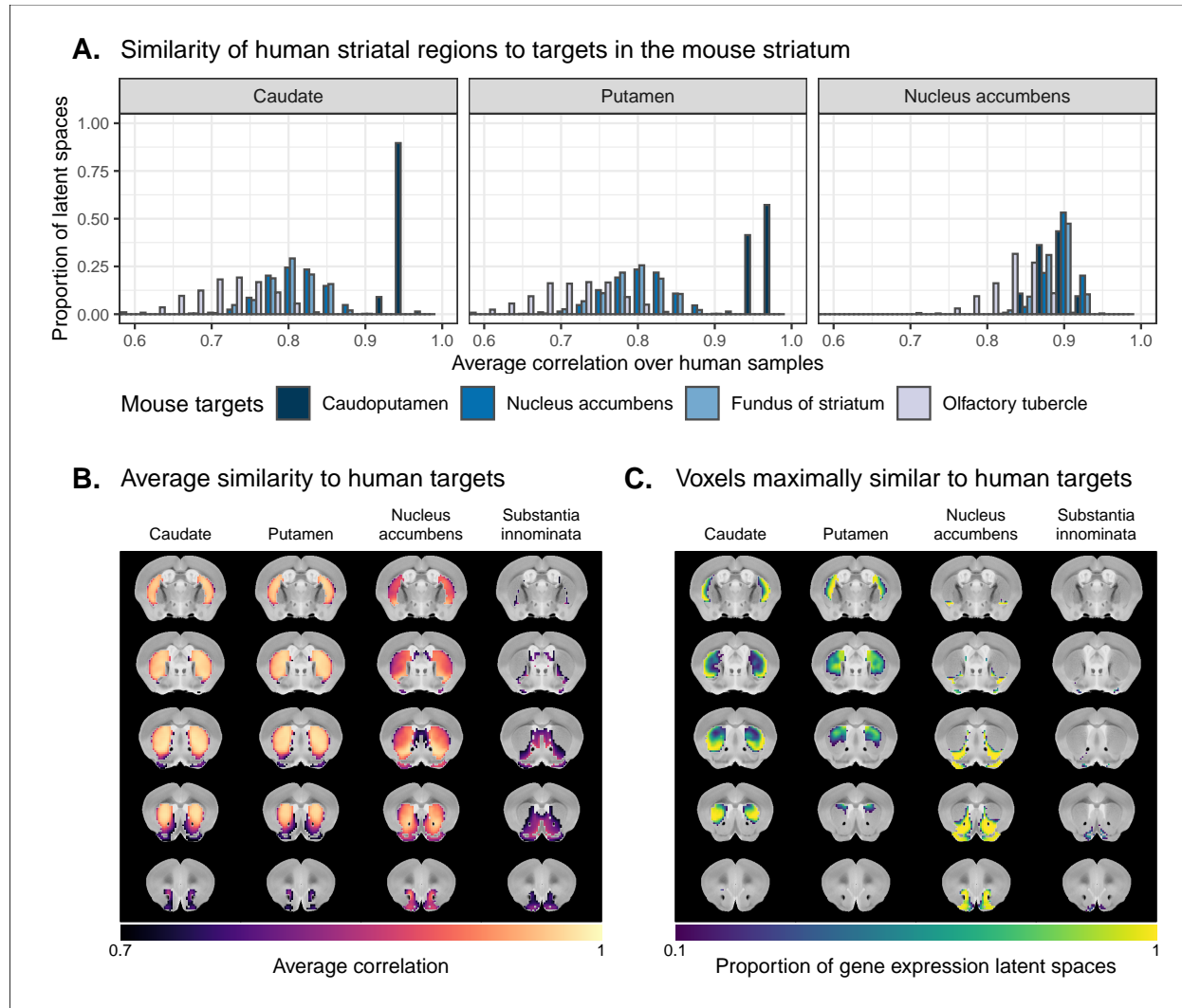


Figure 6. Similarity among mouse and human striatal regions. **(A)** Distributions over gene expression latent spaces of region-wise average correlation values for mouse and human striatal pairs. Human regions were chosen based on the AHBA ontology. Mouse target regions were chosen to be those with the highest average correlation values. **(B)** Latent space averaged correlations between voxels in the mouse striatum and human target regions. Target regions were selected based on the highest mean correlation across all striatal voxels. **(C)** Proportions of latent spaces in which mouse striatal voxels are maximally similar to human target regions. Source data 1. Related to Figure 6A. Source data 2. Related to Figure 6B. Source data 3. Related to Figure 6C. Source data 4. Related to Figure 6C. Source data 5. Related to Figure 6C.

452 Discussion

453 We have demonstrated how spatial transcriptomic patterns of homologous genes can be used to make quan-
 454 titative comparisons between the mouse and human brain. We showed that using homologous genes as a

455 common space allows one to easily identify coarse similarities in brain structures across species, but that
456 more fine-scaled parcellations, such as at the level of cortical areas, are more complex. Despite this limi-
457 tation, the approach still allows for a formal assessment of different patterns of between-species similarity
458 in primary compared to supramodal regions, identifications of distinct clusters of cortical territories across
459 species, and comparison of between-species similarities at the transcriptomic level to those observed using
460 other modalities. We will discuss our observations in the context of the importance of the mouse as a model
461 for human neuroscience below.

462 The abundance of neuroscience research performed using mice has resulted in a wealth of knowledge about the
463 mouse brain. In the preclinical setting, mouse models are utilized with the intention of better understanding
464 human neuropathology. For instance, in the context of autism spectrum disorders, a plethora of studies
465 using mouse models have reported on the neurobiological and neuroanatomical phenotypes that arise from
466 mutations at specific genetic loci (Gompers et al., 2017; Horev et al., 2011; Pagani et al., 2021). It is common
467 for researchers involved in translational neuroscience to rely on findings of this kind to make inferences about
468 the human disorder. The typical approach, which is to identify rough post-hoc correspondences between
469 neuroanatomical ontologies, is not particularly comprehensive and is subject to confirmation bias. While it
470 may be a reasonable starting point for comparison, the true correspondence between the mouse and human
471 brain is likely more complicated given the evolutionary distance between the two species. Although overall
472 patterns of brain organization, including the general pattern of neocortical organization, are similar across
473 all mammals, substantial differences are evident (Ventura-Antunes et al., 2013). To make matters worse,
474 researchers from the different neuroscientific traditions often use distinct terminology, further complicating
475 detailed information exchange. To address these problems, we sought to establish a first quantitative whole-
476 brain comparison between the two species.

477 The expression of homologous genes provides an elegant way to define a common space for quantitative cross-
478 species comparisons since it relies on homology at a deep molecular biological level. The approach is not
479 without limitations however. First, the acquisition of whole-brain transcriptomic data is labour-intensive,
480 time consuming, and invasive. These data sets cannot be generated easily, especially in the human, in which
481 the process depends on the availability of post-mortem samples. As a result, the effective sample sizes are
482 extremely limited in this domain. For instance, in the Allen mouse coronal in-situ hybridization data set
483 used here, the brain-wide expression of each gene is sampled only once (barring a few exceptions). This
484 constrains the types of analyses that are possible (e.g. null hypothesis significance testing) and largely limits
485 the availability of replication data sets. That being said, new technologies, such as spatial transcriptomics,
486 are gradually making it easier to acquire brain-wide gene expression data in less time and at lower cost

487 (Ortiz et al., 2020; Stahl et al., 2016; Vickovic et al., 2019). Second, the approach of relying on all available
488 genes is subject to noise. To address this issue, Myers (Myers, 2017) used a method of gene set selection to
489 attempt to improve the correspondence between established mouse-human homologies. While this lead to
490 improvement, it was only at the level of coarsely defined regions (e.g. isocortex-isocortex). Our approach,
491 therefore, was to use supervised machine learning to create a latent common space based on combinations
492 of homologous genes that can delineate areas within a single species.

493 This latent common space approach led to a substantial improvement in specificity of between-species com-
494 parisons. Nevertheless, it is evident that the first major distinction in gene expression patterns within a
495 species, and the easiest identification of similarity across species, is at the coarse anatomical level of the
496 major subdivisions of the vertebrate brain, such as the isocortex, cerebellar hemispheres and nuclei, and
497 brain stem. All of these territories were present in the ancestral vertebrate brain (Striedter and Northcutt,
498 2020) and the ability to detect conserved transcriptomic signatures at this level is not surprising. Within
499 such structures, such as the isocortex, our ability to make simple one-to-one correspondences decreased. This
500 is partly because areas within a coarse structure have more similar transcriptomic profiles, but also likely
501 due to the fact that a single area in one brain does not have a single correspondent in another, larger brain.
502 In other words, regions in the brains of related species may exhibit one-to-many or many-to-many mappings.
503 In our study, we found greater cross-species similarity between isocortical areas associated with sensorimotor
504 processing than areas in supramodal isocortex. Primary areas, including the sensorimotor areas, are present
505 in all mammals studied to date and likely part of the common ancestors of all mammals (Kaas, 2011a;
506 Krubitzer, 2007). Although this common ancestor likely also had non-primary areas, it cannot be denied
507 that association cortex expanded dramatically in primates and especially so in the human brain (Chaplin et
508 al., 2013; Mars et al., 2016a). Again, the pattern found here of greater similarity in more conserved areas
509 might reflect this evolutionary history. In that context it is interesting to note that some non-primary areas
510 thought to be present in the common mammalian ancestor, such as cingulate and orbitofrontal cortex (Kaas,
511 2011a) showed relatively high correlation to human areas.

512 An advantage of the approach presented here is that it can, in principle, be applied to any aspect of brain
513 organization. Beyond simply establishing whether areas are similar across species in a particular common
514 space, comparing the results across common spaces established using different types of neuronal data can
515 inform on which larger principles of organization are similar across brains (Eichert et al., 2020). This is
516 illustrated here by the results of our striatal analysis. We found high similarity between the human caudate
517 and putamen and mouse caudoputamen, with little differentiation within these regions in a single species.
518 In contrast, Balsters et al. (2020) demonstrated that human caudoputamen contains a distinct pattern of

519 connectivity. At first sight, one could argue the results are in contrast. However, evolutionarily speaking, it
520 is quite probable that an overall similar transcriptomic signature of the striatum can be accompanied by a
521 distinct connectivity pattern to areas of the cortex present in only one of the two species. Indeed, this speaks
522 to the different types of similarity that can be studied, depending on which aspect of brain organization one
523 is interested in. Although the human brain is much larger than the mouse brain and contains a number
524 of cortical territories that have no homologue in the mouse brain (Kaas, 2011b; Rudebeck and Izquierdo,
525 2022), the similarity in transcriptomic signature mean that translations between the species is valid in
526 many contexts. The supervised learning approach also provides interesting avenues for future research. For
527 instance, rather than classifying all regions in the brain at once, separate models could be trained to classify
528 regions belonging to different sub-trees in the neuroanatomical hierarchy (see Figure 5-supplement 1 and
529 Figure 5-supplement 2). This type of approach requires more exploration however, such as where to split
530 the hierarchy, how to optimize the classifiers for each sub-tree, and how to stitch all this information back
531 together at the end in order to make comparisons between different sub-trees.

532 The power of a formal understanding of similarities and differences between brains at different levels of
533 organization is evident. In fundamental neuroscience, it will help translate results from data types that
534 cannot be obtained in humans to the human brain (Barron et al., 2021). In translational neuroscience, it
535 will, in a negative sense, help establish the limits of the translational paradigm by showing which aspects
536 of the human brain cannot be understood using the model species (Liu et al., 2021). In a positive sense,
537 it will also help by establishing and improving our understanding of the many aspects in which the model
538 and human brain do concur (Mandino et al., 2021). More ambitious still, it can provide a way in which
539 highly diverse manifestations of certain disease syndromes (e.g. autism spectrum disorder) (Grzadzinski et
540 al., 2013; Simonoff et al., 2008) and the availability of many distinct model strains (Ellegood et al., 2015),
541 each hypothesized to capture a distinct aspect of a multi-dimensional clinical syndrome, can be related to
542 one another. Ultimately, we believe that using the mapping of homologous gene expression between species
543 can be an important part of building a transform that maps information obtained using mice to humans and
544 vice versa.

545 **Materials and methods**

546 **Mouse gene expression data**

547 We used the adult mouse whole-brain in-situ hybridization data sets from the Allen Mouse Brain Atlas
548 (Lein et al., 2007). Specifically, we used 3D expression grid data, i.e. expression data aligned to the Allen
549 Mouse Brain Common Coordinate Framework (CCFv3)(Wang et al., 2020) and summarized under a grid
550 at a resolution of $200\mu\text{m}$. We downloaded the gene expression “energy” volumes from both the coronal
551 and sagittal in-situ hybridization experiments as a sequence of 32-bit float values using the Allen Institute’s
552 API (<http://help.brain-map.org/display/api/Downloading+3-D+Expression+Grid+Data>). These volumes
553 were subsequently reshaped into 3D images in the MINC format. Origin, extents, and spacing were defined
554 such that the image was RAS-oriented, with the origin at the point where the anterior commissure crosses
555 the midline. The MINC images from the coronal and sagittal data sets were then processed separately
556 using the Python programming language. The sagittal data set was first filtered to keep only those genes
557 that were also present in the coronal set. Images were imported using the `pyminc` package, masked and
558 reshaped to form an experiment-by-voxel expression matrix. We pre-processed this data by first applying a
559 `log2` transformation for consistency with the human data set. For those genes associated with more than
560 one in-situ hybridization experiment, we averaged the expression of each voxel across the experiments. We
561 subsequently filtered out genes for which more than 20% of voxels contained missing values. Finally, we
562 applied a K-nearest neighbours algorithm to impute the remaining missing values. The result of this pre-
563 processing pipeline was a gene-by-voxel expression matrix with 3958 genes and 61315 voxels for the coronal
564 data set and a matrix with 3619 genes and 26317 voxels for the sagittal data set.

565 **Human gene expression data**

566 Human gene expression data was obtained from the Allen Human Brain Atlas (Hawrylycz et al., 2012).
567 The data were downloaded from the Allen Institute’s API (<http://api.brain-map.org>) and pre-processed
568 using the `abagen` package in Python (<https://abagen.readthedocs.io/en/stable/>) (Arnatkevičiūtė et al., 2019;
569 Hawrylycz et al., 2012; Markello et al., 2021). We used the microarray data from the brains of all six donors,
570 each of which contains `log2` expression values for 58692 gene probes across numerous tissue samples. The
571 pre-processing pipeline included probe selection using differential stability on data from all donors and
572 intensity-based filtering of probes at a threshold of 0.5. The samples and genes were additionally normalized
573 for each donor individually using a scaled robust sigmoid function. In practice, this pipeline was implemented

574 using the `get_samples_in_mask` function from the `abagen` package. The remaining parameters were set to
575 their default values. The output of the pre-processing pipeline was a gene-by-sample expression matrix with
576 15627 genes and 3702 samples across all donors.

577 Mouse atlases

578 We used a version of the DSURQE atlas from the Mouse Imaging Centre (Dorr et al., 2008; Qiu et al., 2018;
579 Richards et al., 2011; Steadman et al., 2014; Ullmann et al., 2013), modified using the AMBA hierarchical
580 ontology, which was downloaded from the Allen Institute’s API. The labels of the DSURQE atlas correspond
581 to the leaf node regions in the AMBA ontology, which allowed us to use the hierarchical neuroanatomical
582 tree to aggregate and prune the atlas labels to the desired level of granularity. For the purposes of our
583 analyses, we removed white matter and ventricular regions entirely. The remaining grey matter regions were
584 aggregated up the hierarchy so that the majority of resulting labels contained enough voxels to be classified
585 appropriately by the multi-layer perceptron. In doing so, we maintained approximately the same level of
586 tree depth within a broad region (e.g. cerebellar regions were chosen at the same level of granularity). This
587 resulted in a mouse atlas with 67 grey matter regions. We additionally generated an atlas with 11 broader
588 regions for visualization and annotation purposes.

589 Human atlases

590 We used the hierarchical ontology from the AHBA, which we obtained using the Allen Institute’s API.
591 We aggregated and pruned the neuroanatomical hierarchy to correspond roughly to the level of granularity
592 obtained in our mouse atlas, resulting in 88 human brain regions. We additionally generated a set of 16
593 broad regions for visualization and annotation. White matter and ventricular regions were omitted entirely.

594 Expression matrices and similarity matrices

595 We created the mouse and human gene-by-region expression matrices from the mouse gene-by-voxel and
596 human gene-by-sample expression matrices. First, we intersected the gene sets in these matrices with a
597 list of 3331 homologous genes obtained from the NCBI HomoloGene database (NCBI, 2018), resulting in
598 2835 homologous genes present in both the mouse and human expression matrices. We then annotated each
599 of the human samples with one of the 88 human atlas regions, and each of the mouse voxels with one of
600 the 67 mouse atlas regions, discarding white matter and ventricular entries in the process. These labelled

601 expression matrices were subsequently normalized as follows: For each matrix, we first normalized each
602 voxel/sample across all homologous genes using a z-scoring procedure to create a normalized gene expression
603 signature for each voxel/sample. We then centered the distribution of expression signatures in gene space
604 by subtracting the mean expression of each homologous gene over all voxels/samples. Finally, we generated
605 the aggregated gene-by-region expression matrices by averaging the normalized expression of every gene over
606 the voxels/samples corresponding to each atlas region. Using these expression matrices, we generated the
607 mouse-human similarity matrix by computing the Pearson correlation coefficient between all pairs of mouse
608 and human regions.

609 Gene enrichment analysis

610 We ran a gene enrichment analysis on the set of homologous genes obtained from the NCBI HomoloGene
611 database. We first downloaded Gene Ontology data for biological process related modules from the Bader
612 Lab at the University of Toronto (<http://baderlab.org/GeneSets>). These data include a gene set of 16563
613 genes and a module set of 15757 biological process modules. Every module is associated with a subset
614 of genes from the full gene set. For each module, we used a hypergeometric test to evaluate whether the
615 homologous gene set was over-represented in the module subset, compared with the full gene set. The
616 resulting p-values were adjusted for multiple comparisons using the false-discovery rate method (Benjamini
617 and Hochberg, 1995). A total of 938 modules were found to be significant at a threshold of 0.001. The
618 surviving modules were ordered according to their p-values and written out to a comma-separated values
619 data file (Supplementary File 1). This analysis was carried out using the `tmod` package in the R programming
620 language.

621 Multi-layer perceptron classification and latent space

622 To improve the resolution of mouse-human neuroanatomical matches, we performed a supervised learning
623 approach, wherein we trained a multi-layer perceptron neural network to classify 67 mouse atlas regions
624 from the expression values of 2835 homologous genes. We chose a model architecture in which each layer of
625 the network was fully connected to previous and subsequent layers. To optimize the hyperparameters, we
626 implemented an ad hoc cross-validation procedure that took into account the fact that the majority of genes
627 in the coronal AMBA data set are sampled only once over the entire mouse brain. The procedure involved
628 a combination of the coronal and the sagittal in-situ hybridization data sets. For the sagittal data set, we
629 used the expression matrix described above. However, we used a modified version of the coronal expression

630 matrix. This matrix was generated using the pipeline described above with the following modifications: 1.
631 We applied the *unilateral* brain mask from the sagittal data set to the coronal images in order to have the
632 same spatial extent, and 2. we did not aggregate the expression of multiple in-situ hybridization experiments
633 for those genes in the coronal set that were measured more than once. We then filtered these voxel-wise
634 expression matrices according to the list of mouse-human homologous genes, as well as the human sample
635 expression matrix. We also annotated the voxels in each of the expression matrices with one of the 67
636 regions in the mouse atlas. Our validation procedure then involved iterative construction of training and
637 validation sets by sampling gene experiments from either the coronal or sagittal matrices. Specifically, for
638 every gene in the homologous set, we first determined whether that gene was associated with more than one
639 experiment in the coronal matrix. If this was the case, we randomly sampled one of those experiments for
640 the training set and one of the remaining experiments for the validation set. If the gene was associated with
641 only one experiment in the coronal set, we randomly sampled either the coronal or sagittal experiment for
642 the training set and the other for the validation set. Once the training and validation sets were generated,
643 they were normalized using the procedure described above. We then optimized the neural network using the
644 training set and evaluated its performance on the validation set. We repeated this construction, training,
645 and validation procedure 5 times for every combination of hyperparameters.

646 Using this validation approach, we tuned the number of hidden layers in the network, the number of hidden
647 units per hidden layer, the amount of weight decay, the maximum learning rate, and the optimization method.
648 The values we sampled were as follows:

- 649 • Number of hidden layers: 3, 4, 5
- 650 • Number of hidden units: 200, 500, 1000
- 651 • Weight decay: 0, 10^{-6} , 10^{-3}
- 652 • Maximum learning rate: 10^{-5} , 10^{-4} , 10^{-3} , 10^{-2} , 10^{-6} , 10^{-1}
- 653 • Optimizer: SGD, AdamW

654 All models were trained over 200 epochs using a one-cycle learning rate policy. The activation function used
655 in the forward pass was the rectified linear unit (ReLU) and the loss function was the negative log-likelihood
656 loss. We found that the best-performing model had 3 hidden layers, 200 neurons per layer, and no weight
657 decay. It was optimized using the AdamW optimization algorithm (Loshchilov and Hutter, 2019) with a
658 maximum learning rate of 10^{-5} . This model returned an average loss of 0.215 on the training sets and
659 of 1.224 on the validation sets. The average training classification accuracy was 0.936 and the validation
660 accuracy was 0.597.

661 Using the optimal hyperparameters, we trained the multi-layer perceptron on the full bilateral coronal voxel-
662 wise expression matrix. We used the trained network to generate the latent gene expression space. To extract
663 the appropriate transformation, we removed the predictive output layer and soft-max transformation from
664 the network architecture. The resulting architecture returns the 200 hidden units in the third hidden layer
665 as the output of the model. To create the latent space data representations, we applied this network to
666 the mouse and human regional and voxel-/sample-wise expression matrices. The resulting matrices have
667 200 columns corresponding to the hidden units and rows corresponding to the number of regions, voxels,
668 or samples in the mouse and human matrices. This process was repeated 500 times to generate 500 latent
669 spaces.

670 These models were implemented in Python using PyTorch (<https://pytorch.org>) and the `skorch` package
671 (<https://skorch.readthedocs.io/en/stable/>).

672 Multi-layer perceptron feature importance

673 We used integrated gradients to evaluate the contribution of different genes in the classification of mouse
674 atlas labels. Since the homologous gene inputs contribute to the classification of distinct labels in different
675 ways, we examined the feature attributions for three regions: the caudoputamen, the primary motor area,
676 and the infralimbic area. Using the trained multi-layer perceptron, we computed integrated gradients for
677 each of these three regions. We then averaged the values over all input voxels for each gene, resulting in a
678 vector of gene attributions for each of the three example regions. This process was repeated for 200 training
679 runs of the neural network. We then averaged the gene importance vectors of each region over all training
680 runs to get a summary of gene importance. This process was implemented using the `IntegratedGradients`
681 function from the `captum` package in Python (<https://captum.ai/>).

682 Statistical modelling

683 To quantify the improvement in the mouse-human matches when using the latent spaces versus the original
684 gene expression space (Figures 3 and 4), we used a set of logistic regression models to estimate the probability
685 that the rank difference was less than or equal to zero. To estimate the overall improvement due to the latent
686 spaces, we created a binary variable to encode whether the average rank difference over latent spaces for
687 each region met the success criterion. This variable was then used as our target in a logistic regression with
688 no regressors. Once the model was fit, we applied the logistic function to the intercept parameter estimate
689 to get the corresponding estimate for the Bernoulli probability, p_B . This transformation was also applied to

690 the bounds on the variance estimate for the intercept to get the corresponding confidence interval. Using the
691 estimated Bernoulli probability, we calculated the corresponding number of successes, k . We then evaluated
692 the probability of obtaining at least k successful outcomes under the null binomial distribution, $B(n, 0.5)$.
693 The parameter n was taken to be the number of brain regions under consideration. We additionally applied
694 this approach on a region-wise basis to evaluate the likelihood of a region seeing improvement in the latent
695 spaces. In this case, the null distribution was $B(500, 0.5)$ for each region. The resulting p-values were
696 adjusted for multiple comparisons using the false-discovery rate method (Benjamini and Hochberg, 1995).
697 These models were implemented using the `glm` function from the `stats` package in the R programming
698 language.

699 In our comparison of sensorimotor and supramodal cortical regions (Figure 5), we used linear models to
700 evaluate the impact of cortex type on maximal correlation values. In the first instance, we computed each
701 region's average maximal correlation over all latent spaces. We then regressed those average values against a
702 binary variable indicating whether the regions were sensorimotor or supramodal. Here we used a simple linear
703 regression. In the second instance, for each latent space we computed average maximal correlation values
704 for sensorimotor regions and supramodal regions. We then regressed these average values against a binary
705 variable as described above. In this case we used a linear mixed-effects regression with a random intercept
706 term to control for observations coming from the same latent space. These models were implemented in
707 the R programming language. The simple linear regression was implemented using the `lm` function from
708 the `stats` package, while the linear mixed-effects regression was implemented using the `lmer` function from
709 the `lme4` package. The `lmerTest` package was used to estimate the degrees of freedom in the mixed-effects
710 model and perform hypothesis testing.

711 Data and code availability

712 This manuscript and all figures were generated programmatically using R Markdown (<https://rmarkdown.rstudio.com>) and L^AT_EX(<https://www.latex-project.org>). The Allen Mouse Brain Atlas and Allen Human
713 Brain Atlas data sets are openly accessible and can be downloaded from the Allen Institute's API (<http://api.brain-map.org>). All of the code and additional data needed to generate this analysis, including figures
714 and manuscript, is accessible at <https://github.com/abeaucha/MouseHumanTranscriptomicSimilarity/>.
715

717 **Acknowledgments**

718 We thank C. Hammill, D.J. Fernandes, E. Anagnostou, B.J. Nieman, and E. Sibille for providing advice
719 and for interesting conceptual discussions. This study was supported by the Canadian Institutes of Health
720 Research (doctoral funding and foreign study award for A.B.). The Wellcome Centre for Integrative Neu-
721 roimaging is supported by core funding from the Wellcome Trust (203139/Z/16/Z).

722 **Competing interests**

723 The authors declare that they have no competing interests.

724 **References**

- 725 Arnatkeviciūtė A, Fulcher BD, Fornito A. 2019. A practical guide to linking brain-wide gene expression and
726 neuroimaging data. *NeuroImage* **189**:353–367. doi:10.1016/j.neuroimage.2019.01.011
- 727 Balsters JH, Zerbi V, Sallet J, Wenderoth N, Mars RB. 2020. Primate homologs of mouse cortico-striatal
728 circuits. *eLife* **9**:24. doi:10.7554/eLife.53680
- 729 Barron HC, Mars RB, Dupret D, Lerch JP, Sampaio-Baptista C. 2021. Cross-species neuroscience:
730 Closing the explanatory gap. *Philosophical Transactions of the Royal Society B: Biological Sciences*
731 **376**:20190633. doi:10.1098/rstb.2019.0633
- 732 Benjamini Y, Hochberg Y. 1995. Controlling the False Discovery Rate: A Practical and Powerful Approach
733 to Multiple Testing. *Journal of the Royal Statistical Society Series B (Methodological)* **57**:289–300.
- 734 Burt JB, Demirtaş M, Eckner WJ, Navejar NM, Ji JL, Martin WJ, Bernacchia A, Anticevic A, Murray JD.
735 2018. Hierarchy of transcriptomic specialization across human cortex captured by structural neuroimag-
736 ing topography. *Nature Neuroscience* **21**:1251–1259. doi:10.1038/s41593-018-0195-0
- 737 Chaplin TA, Yu H-H, Soares JGM, Gattass R, Rosa MGP. 2013. A Conserved Pattern of Differen-
738 tial Expansion of Cortical Areas in Simian Primates. *Journal of Neuroscience* **33**:15120–15125.
739 doi:10.1523/JNEUROSCI.2909-13.2013
- 740 Dietrich MR, Ankeny RA, Chen PM. 2014. Publication Trends in Model Organism Research. *Genetics*
741 **198**:787–794. doi:10.1534/genetics.114.169714
- 742 Dorr AE, Lerch JP, Spring S, Kabani N, Henkelman RM. 2008. High resolution three-dimensional brain
743 atlas using an average magnetic resonance image of 40 adult C57Bl/6J mice. *NeuroImage* **42**:60–69.
744 doi:10.1016/j.neuroimage.2008.03.037

- 745 Eichert N, Robinson EC, Bryant KL, Jbabdi S, Jenkinson M, Li L, Krug K, Watkins KE, Mars RB. 2020.
746 Cross-species cortical alignment identifies different types of anatomical reorganization in the primate
747 temporal lobe. *eLife* **9**:e53232. doi:10.7554/eLife.53232
- 748 Ellegood J, Anagnostou E, Babineau BA, Crawley JN, Lin L, Genestine M, DiCicco-Bloom E, Lai JK, Y,
749 Foster JA, Peñagarikano O, Geschwind DH, Pacey LK, Hampson DR, Laliberté CL, Mills AA, Tam
750 E, Osborne LR, Kouwer M, Espinosa-Becerra F, Xuan Z, Powell CM, Raznahan A, Robins DM, Nakai
751 N, Nakatani J, Takumi T, Eede MC van, Kerr TM, Muller C, Blakely RD, Veenstra-VanderWeele J,
752 Henkelman RM, Lerch JP. 2015. Clustering autism: Using neuroanatomical differences in 26 mouse
753 models to gain insight into the heterogeneity. *Molecular Psychiatry* **20**:118–125. doi:10.1038/mp.2014.98
- 754 Ellenbroek B, Youn J. 2016. Rodent models in neuroscience research: Is it a rat race? *Disease Models &*
755 *Mechanisms* **9**:1079–1087. doi:10.1242/dmm.026120
- 756 Englund M, James SS, Bottom R, Huffman KJ, Wilson SP, Krubitzer LA. 2021. Comparing cortex-wide
757 gene expression patterns between species in a common reference frame. doi:10.1101/2021.07.28.454203
- 758 Fulcher BD, Murray JD, Zerbi V, Wang X-J. 2019. Multimodal gradients across mouse cortex. *Proceedings*
759 *of the National Academy of Sciences* **116**:4689–4695. doi:10.1073/pnas.1814144116
- 760 Gompers AL, Su-Feher L, Ellegood J, Copping NA, Riyadh MA, Stradleigh TW, Pride MC, Schaffler MD,
761 Wade AA, Catta-Preta R, Zdilar I, Louis S, Kaushik G, Mannion BJ, Plajzer-Frick I, Afzal V, Visel
762 A, Pennacchio LA, Dickel DE, Lerch JP, Crawley JN, Zarbalis KS, Silverman JL, Nord AS. 2017.
763 Germline Chd8 haploinsufficiency alters brain development in mouse. *Nature Neuroscience* **20**:1062–
764 1073. doi:10.1038/nn.4592
- 765 Grzadzinski R, Huerta M, Lord C. 2013. DSM-5 and autism spectrum disorders (ASDs): An opportunity
766 for identifying ASD subtypes. *Molecular Autism* **4**:12. doi:10.1186/2040-2392-4-12
- 767 Hawrylycz MJ, Lein ES, Guillozet-Bongaarts AL, Shen EH, Ng L, Miller JA, Lagemaat LN van de, Smith
768 KA, Ebbert A, Riley ZL, Abajian C, Beckmann CF, Bernard A, Bertagnolli D, Boe AF, Cartagena PM,
769 Chakravarty MM, Chapin M, Chong J, Dalley RA, Daly BD, Dang C, Datta S, Dee N, Dolbeare TA, Faber
770 V, Feng D, Fowler DR, Goldy J, Gregor BW, Haradon Z, Haynor DR, Hohmann JG, Horvath S, Howard
771 RE, Jeromin A, Jochim JM, Kinnunen M, Lau C, Lazarz ET, Lee C, Lemon TA, Li L, Li Y, Morris JA,
772 Overly CC, Parker PD, Parry SE, Reding M, Royall JJ, Schulkin J, Sequeira PA, Slaughterbeck CR, Smith
773 SC, Sodt AJ, Sunkin SM, Swanson BE, Vawter MP, Williams D, Wohnoutka P, Zielke HR, Geschwind
774 DH, Hof PR, Smith SM, Koch C, Grant SGN, Jones AR. 2012. An anatomically comprehensive atlas of
775 the adult human brain transcriptome. *Nature* **489**:391–399. doi:10.1038/nature11405
- 776 Hay M, Thomas DW, Craighead JL, Economides C, Rosenthal J. 2014. Clinical development success rates
777 for investigational drugs. *Nature Biotechnology* **32**:40–51. doi:10.1038/nbt.2786

- 778 Hedrich HJ, Mossmann H, Nicklas W. 2004. Chapter 24: Housing and maintenanceThe Laboratory Mouse.
779 Elsevier Academic Press. pp. 395–408.
- 780 Heukelum S van, Mars RB, Guthrie M, Buitelaar JK, Beckmann CF, Tiesinga PHE, Vogt BA, Glennon
781 JC, Havenith MN. 2020. Where is Cingulate Cortex? A Cross-Species View. *Trends in Neurosciences*
782 **43**:285–299. doi:10.1016/j.tins.2020.03.007
- 783 Hodge RD, Bakken TE, Miller JA, Smith KA, Barkan ER, Graybuck LT, Close JL, Long B, Johansen N,
784 Penn O, Yao Z, Eggermont J, Höllt T, Levi BP, Shehata SI, Aevermann B, Beller A, Bertagnolli D,
785 Brouner K, Casper T, Cobbs C, Dalley R, Dee N, Ding S-L, Ellenbogen RG, Fong O, Garren E, Goldy
786 J, Gwinn RP, Hirschstein D, Keene CD, Keshk M, Ko AL, Lathia K, Mahfouz A, Maltzer Z, McGraw
787 M, Nguyen TN, Nyhus J, Ojemann JG, Oldre A, Parry S, Reynolds S, Rimorin C, Shapovalova NV,
788 Somasundaram S, Szafer A, Thomsen ER, Tieu M, Quon G, Scheuermann RH, Yuste R, Sunkin SM,
789 Lelieveldt B, Feng D, Ng L, Bernard A, Hawrylycz M, Phillips JW, Tasic B, Zeng H, Jones AR, Koch
790 C, Lein ES. 2019. Conserved cell types with divergent features in human versus mouse cortex. *Nature*
791 **573**:61–68. doi:10.1038/s41586-019-1506-7
- 792 Horev G, Ellegood J, Lerch JP, Son Y-EE, Muthuswamy L, Vogel H, Krieger AM, Buja A, Henkelman RM,
793 Wigler M, Mills AA. 2011. Dosage-dependent phenotypes in models of 16p11.2 lesions found in autism.
794 *Proceedings of the National Academy of Sciences* **108**:17076–17081. doi:10.1073/pnas.1114042108
- 795 Houdebine L-M. 2004. Chapter 6: The mouse as an animal model for human diseasesThe Laboratory Mouse.
796 Elsevier Academic Press. pp. 97–107.
- 797 Kaas JH. 2012. The evolution of neocortex in primates. *Progress in brain research* **195**:91–102.
798 doi:10.1016/B978-0-444-53860-4.00005-2
- 799 Kaas JH. 2011a. Reconstructing the Areal Organization of the Neocortex of the First Mammals. *Brain,*
800 *Behavior and Evolution* **78**:7–21. doi:10.1159/000327316
- 801 Kaas JH. 2011b. Neocortex in early mammals and its subsequent variations. *Annals of the New York*
802 *Academy of Sciences* **1225**:10.1111/j.1749–6632.2011.05981.x. doi:10.1111/j.1749-6632.2011.05981.x
- 803 Krubitzer L. 2007. The Magnificent Compromise: Cortical Field Evolution in Mammals. *Neuron* **56**:201–
804 208. doi:10.1016/j.neuron.2007.10.002
- 805 Laubach M, Amarante LM, Swanson K, White SR. 2018. What, If Anything, Is Rodent Prefrontal Cortex?
806 *eneuro* **5**:ENEURO.0315–18.2018. doi:10.1523/ENEURO.0315-18.2018
- 807 Lein ES, Hawrylycz MJ, Ao N, Ayres M, Bensinger A, Bernard A, Boe AF, Boguski MS, Brockway KS,
808 Byrnes EJ, Chen L, Chen L, Chen T-M, Chi Chin M, Chong J, Crook BE, Czaplinska A, Dang CN,
809 Datta S, Dee NR, Desaki AL, Desta T, Diep E, Dolbeare TA, Donelan MJ, Dong H-W, Dougherty JG,
810 Duncan BJ, Ebbert AJ, Eichele G, Estin LK, Faber C, Facer BA, Fields R, Fischer SR, Fliss TP, Frenslay

- 811 C, Gates SN, Glattfelder KJ, Halverson KR, Hart MR, Hohmann JG, Howell MP, Jeung DP, Johnson
812 RA, Karr PT, Kawal R, Kidney JM, Knapik RH, Kuan CL, Lake JH, Laramee AR, Larsen KD, Lau C,
813 Lemon TA, Liang AJ, Liu Y, Luong LT, Michaels J, Morgan JJ, Morgan RJ, Mortrud MT, Mosqueda
814 NF, Ng LL, Ng R, Orta GJ, Overly CC, Pak TH, Parry SE, Pathak SD, Pearson OC, Puchalski RB,
815 Riley ZL, Rockett HR, Rowland SA, Royall JJ, Ruiz MJ, Sarno NR, Schaffnit K, Shapovalova NV,
816 Sivisay T, Slaughterbeck CR, Smith SC, Smith KA, Smith BI, Sodt AJ, Stewart NN, Stumpf K-R,
817 Sunkin SM, Sutram M, Tam A, Teemer CD, Thaller C, Thompson CL, Varnam LR, Visel A, Whitlock
818 RM, Wohynoutka PE, Wolkey CK, Wong VY, Wood M, Yaylaoglu MB, Young RC, Youngstrom BL, Feng
819 Yuan X, Zhang B, Zwingman TA, Jones AR. 2007. Genome-wide atlas of gene expression in the adult
820 mouse brain. *Nature* **445**:168–176. doi:10.1038/nature05453
- 821 Liu X, Eickhoff SB, Caspers S, Wu J, Genon S, Hoffstaedter F, Mars RB, Sommer IE, Eickhoff CR, Chen
822 J, Jardri R, Reetz K, Dogan I, Aleman A, Kogler L, Gruber O, Caspers J, Mathys C, Patil KR. 2021.
823 Functional parcellation of human and macaque striatum reveals human-specific connectivity in the dorsal
824 caudate. *NeuroImage* **235**:118006. doi:10.1016/j.neuroimage.2021.118006
- 825 Loshchilov I, Hutter F. 2019. Decoupled Weight Decay RegularizationProceedings of the Seventh Interna-
826 tional Conference on Learning Representations. New Orleans.
- 827 Mandino F, Vrooman RM, Foo HE, Yeow LY, Bolton TAW, Salvan P, Teoh CL, Lee CY, Beauchamp A, Luo
828 S, Bi R, Zhang J, Lim GHT, Low N, Sallet J, Gigg J, Lerch JP, Mars RB, Olivo M, Fu Y, Grandjean J.
829 2021. A triple-network organization for the mouse brain. *Molecular Psychiatry* 1–8. doi:10.1038/s41380-
830 021-01298-5
- 831 Markello RD, Arnatkevičiūtė A, Poline J-B, Fulcher BD, Fornito A. 2021. Standardizing workflows in
832 imaging transcriptomics with the abagen toolbox. *Biorxiv* 22.
- 833 Mars RB, Jbabdi S, Rushworth MFS. 2021. A Common Space Approach to Comparative Neuroscience.
834 *Annual Review of Neuroscience* **44**:69–86. doi:10.1146/annurev-neuro-100220-025942
- 835 Mars Rogier B, Passingham RE, Jbabdi S. 2018a. Connectivity Fingerprints: From Areal Descriptions to
836 Abstract Spaces. *Trends in Cognitive Sciences* **22**:1026–1037. doi:10.1016/j.tics.2018.08.009
- 837 Mars RB, Passingham RE, Neubert F-X, Verhagen L, Sallet J. 2016a. Evolutionary specializations of human
838 association cortexEvolution of Nervous Systems. Academic Press. pp. 185–205.
- 839 Mars RB, Sallet J, Neubert F-X, Rushworth MFS. 2013. Connectivity profiles reveal the relationship between
840 brain areas for social cognition in human and monkey temporoparietal cortex. *Proceedings of the National
841 Academy of Sciences* **110**:10806–10811. doi:10.1073/pnas.1302956110
- 842 Mars Rogier B, Sotiropoulos SN, Passingham RE, Sallet J, Verhagen L, Khrapitchev AA, Sibson N, Jbabdi S.
843 2018b. Whole brain comparative anatomy using connectivity blueprints. *eLife* **7**. doi:10.7554/eLife.35237

- 844 Mars RB, Verhagen L, Gladwin TE, Neubert F-X, Sallet J, Rushworth MFS. 2016b. Comparing brains by matching connectivity profiles. *Neuroscience & Biobehavioral Reviews* **60**:90–97. doi:10.1016/j.neubiorev.2015.10.008
- 847 Myers E. 2017. Molecular neuroanatomy: Mouse-human homologies and the landscape of genes implicated in language disorders (PhD thesis). Boston University.
- 849 NCBI. 2018. Database resources of the National Center for Biotechnology Information. *Nucleic Acids Research* **46**:D8–D13. doi:10.1093/nar/gkx1095
- 851 Neubert F-X, Mars RB, Thomas AG, Sallet J, Rushworth MFS. 2014. Comparison of Human Ventral Frontal Cortex Areas for Cognitive Control and Language with Areas in Monkey Frontal Cortex. *Neuron* **81**:700–713. doi:10.1016/j.neuron.2013.11.012
- 854 Oh SW, Harris JA, Ng L, Winslow B, Cain N, Mihalas S, Wang Q, Lau C, Kuan L, Henry AM, Mortrud MT, Ouellette B, Nguyen TN, Sorensen SA, Slaughterbeck CR, Wakeman W, Li Y, Feng D, Ho A, Nicholas E, Hirokawa KE, Bohn P, Joines KM, Peng H, Hawrylycz MJ, Phillips JW, Hohmann JG, Wohynoutka P, Gerfen CR, Koch C, Bernard A, Dang C, Jones AR, Zeng H. 2014. A mesoscale connectome of the mouse brain. *Nature* **508**:207–214. doi:10.1038/nature13186
- 856 Ortiz C, Fernandez Navarro J, Jurek A, Martin A, Lundeberg J, Meletis K. 2020. Molecular atlas of the adult mouse brain. *Science Advances* **6**:14.
- 861 Pagani M, Barsotti N, Bertero A, Trakoshis S, Ulysse L, Locarno A, Miseviciute I, De Felice A, Canella C, Supekar K, Galbusera A, Menon V, Tonini R, Deco G, Lombardo MV, Pasqualetti M, Gozzi A. 2021. mTOR-related synaptic pathology causes autism spectrum disorder-associated functional hyperconnectivity. *Nature Communications* **12**:6084. doi:10.1038/s41467-021-26131-z
- 865 Passingham RE, Stephan KE, Kotter R. 2002. The anatomical basis of functional localization in the cortex. *Nature Reviews Neuroscience* **3**:606–616. doi:10.1038/nrn893
- 867 Preuss TM. 1995. Do rats have prefrontal cortex? The Rose-Woolsey-Akert program reconsidered. *Journal of Cognitive Neuroscience* **7**:24.
- 869 Qiu LR, Fernandes DJ, Szulc-Lerch KU, Dazai J, Nieman BJ, Turnbull DH, Foster JA, Palmert MR, Lerch JP. 2018. Mouse MRI shows brain areas relatively larger in males emerge before those larger in females. *Nature Communications* **9**:2615. doi:10.1038/s41467-018-04921-2
- 872 Richards K, Watson C, Buckley RF, Kurniawan ND, Yang Z, Keller MD, Beare R, Bartlett PF, Egan GF, Galloway GJ, Paxinos G, Petrou S, Reutens DC. 2011. Segmentation of the mouse hippocampal formation in magnetic resonance images. *NeuroImage* **58**:732–740. doi:10.1016/j.neuroimage.2011.06.025
- 875 Rudebeck PH, Izquierdo A. 2022. Foraging with the frontal cortex: A cross-species evaluation of reward-guided behavior. *Neuropsychopharmacology* **47**:134–146. doi:10.1038/s41386-021-01140-0

- 877 Sallet J, Mars RB, Noonan MP, Neubert F-X, Jbabdi S, O'Reilly JX, Filippini N, Thomas AG, Rushworth
878 MF. 2013. The Organization of Dorsal Frontal Cortex in Humans and Macaques. *Journal of Neuroscience*
879 **33**:12255–12274. doi:10.1523/JNEUROSCI.5108-12.2013
- 880 Schaeffer DJ, Hori Y, Gilbert KM, Gati JS, Menon RS, Everling S. 2020. Divergence of rodent and pri-
881 mate medial frontal cortex functional connectivity. *Proceedings of the National Academy of Sciences*
882 **117**:21681–21689. doi:10.1073/pnas.2003181117
- 883 Simonoff E, Pickles A, Charman T, Chandler S, Loucas T, Baird G. 2008. Psychiatric Disorders in Children
884 With Autism Spectrum Disorders: Prevalence, Comorbidity, and Associated Factors in a Population-
885 Derived Sample. *Journal of the American Academy of Child & Adolescent Psychiatry* **47**:921–929.
886 doi:10.1097/CHI.0b013e318179964f
- 887 Stahl PL, Salmén F, Vickovic S, Lundmark A, Navarro JF, Magnusson J, Giacomello S, Asp M, Westholm
888 JO, Huss M, Mollbrink A, Linnarsson S, Codeluppi S, Borg Å, Pontén F, Costea PI, Sahlén P, Mulder
889 J, Bergmann O, Lundeberg J, Frisén J. 2016. Visualization and analysis of gene expression in tissue
890 sections by spatial transcriptomics. *Science* **353**:78–82. doi:10.1126/science.aaf2403
- 891 Steadman PE, Ellegood J, Szulc KU, Turnbull DH, Joyner AL, Henkelman RM, Lerch JP. 2014. Genetic
892 Effects on Cerebellar Structure Across Mouse Models of Autism Using a Magnetic Resonance Imaging
893 Atlas: MRI of genetic mouse model's cerebellum. *Autism Research* **7**:124–137. doi:10.1002/aur.1344
- 894 Striedter GF, Northcutt RG. 2020. Brains Through Time. Oxford University Press.
- 895 Sundararajan M, Taly A, Yan Q. 2017. Axiomatic Attribution for Deep NetworksProceedings of the 34th
896 International Conference on Machine Learning. PMLR. pp. 3319–3328.
- 897 Ullmann JFP, Watson C, Janke AL, Kurniawan ND, Reutens DC. 2013. A segmentation protocol and MRI
898 atlas of the C57BL/6J mouse neocortex. *NeuroImage* **78**:196–203. doi:10.1016/j.neuroimage.2013.04.008
- 899 Ventura-Antunes L, Mota B, Herculano-Houzel S. 2013. Different scaling of white matter volume, cor-
900 tical connectivity, and gyration across rodent and primate brains. *Frontiers in Neuroanatomy* **7**.
901 doi:10.3389/fnana.2013.00003
- 902 Vickovic S, Eraslan G, Salmén F, Klughammer J, Stenbeck L, Schapiro D, Äijö T, Bonneau R, Bergenstråhlé
903 L, Navarro JF, Gould J, Griffin GK, Borg Å, Ronaghi M, Frisén J, Lundeberg J, Regev A, Ståhl PL.
904 2019. High-definition spatial transcriptomics for *in situ* tissue profiling. *Nature methods* **16**:987–990.
905 doi:10.1038/s41592-019-0548-y
- 906 Wang Q, Ding S-L, Li Y, Royall J, Feng D, Lesnar P, Graddis N, Naeemi M, Facer B, Ho A, Dolbeare T,
907 Blanchard B, Dee N, Wakeman W, Hirokawa KE, Szafer A, Sunkin SM, Oh SW, Bernard A, Phillips
908 JW, Hawrylycz M, Koch C, Zeng H, Harris JA, Ng L. 2020. The Allen Mouse Brain Common Coordinate
909 Framework: A 3D Reference Atlas. *Cell* **181**:936–953.e20. doi:10.1016/j.cell.2020.04.007

910 Yao Z, Velthoven CTJ van, Nguyen TN, Goldy J, Sedeno-Cortes AE, Baftizadeh F, Bertagnolli D, Casper
 911 T, Chiang M, Crichton K, Ding S-L, Fong O, Garren E, Glandon A, Gouwens NW, Gray J, Graybuck
 912 LT, Hawrylycz MJ, Hirschstein D, Kroll M, Lathia K, Lee C, Levi B, McMillen D, Mok S, Pham T,
 913 Ren Q, Rimorin C, Shapovalova N, Sulc J, Sunkin SM, Tieu M, Torkelson A, Tung H, Ward K, Dee N,
 914 Smith KA, Tasic B, Zeng H. 2021. A taxonomy of transcriptomic cell types across the isocortex and
 915 hippocampal formation. *Cell* **184**:3222–3241.e26. doi:10.1016/j.cell.2021.04.021

916 **Figure supplements**

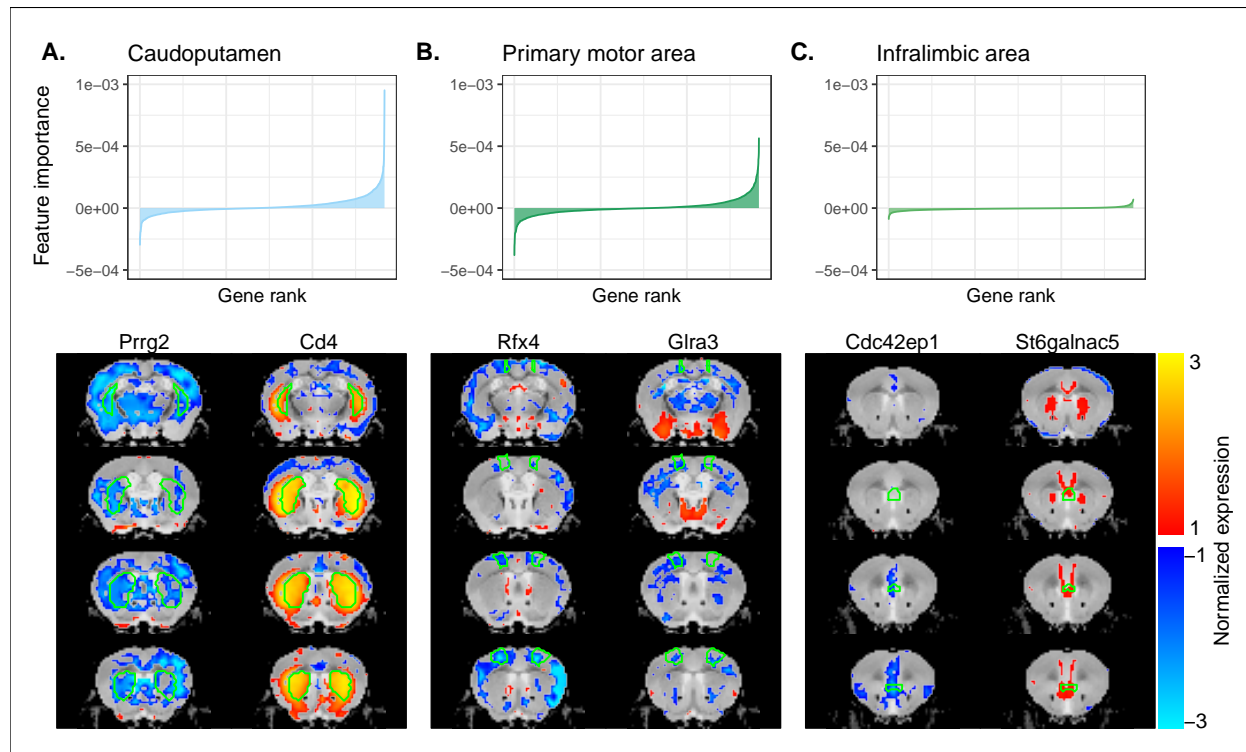


Figure 2-figure supplement 1. Multi-layer perceptron feature importance for the classification of the caudoputamen (**A**), the primary motor area (**B**), and the infralimbic area (**C**). Top row: Rank-ordered distributions of feature importance for the three example regions, averaged over 200 training runs. While the perceptron relies on information from all input genes, a reduced subset of genes is often more informative for the classification of a given label. Bottom row: Coronal slice series displaying the normalized expression patterns for the two genes most informative in the classification of example regions. The spatial expression patterns can be specific to the region of interest, but this is not necessarily the case.

917 **Source data files**

- 918 • Figure 1 - Source data 1: Mouse-human similarity matrix using homologous genes.
 919 • Figure 2 - Source data 1: Correlations between mouse and human brain regions in all latent spaces (1
 920 of 3).

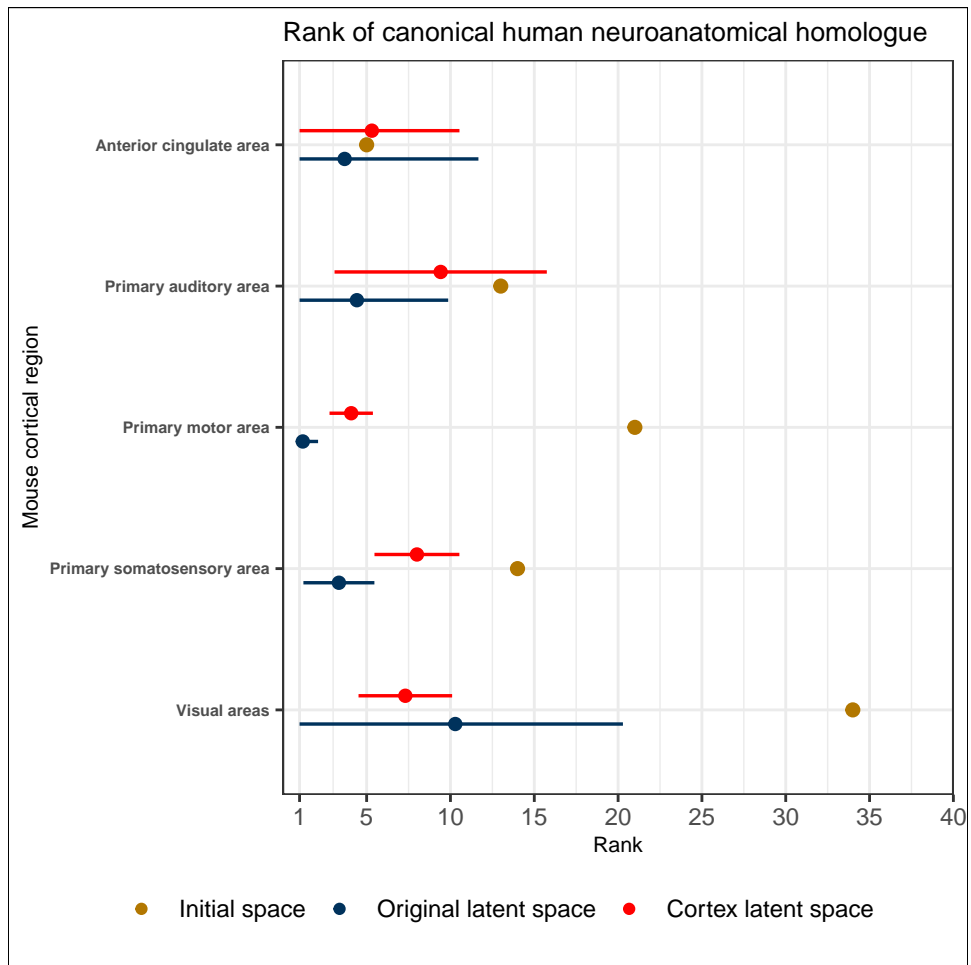


Figure 5-figure supplement 1. Comparison between the ranks of canonical human matches for mouse cortical seed regions in various gene expression spaces. Points and error bars represent mean and 95% confidence interval. Intervals are truncated at a minimal rank of 1. The original latent spaces are the latent spaces obtained from classifying all 67 mouse brain regions. The cortex latent spaces are the latent spaces obtained from classifying 19 mouse cortical regions only.

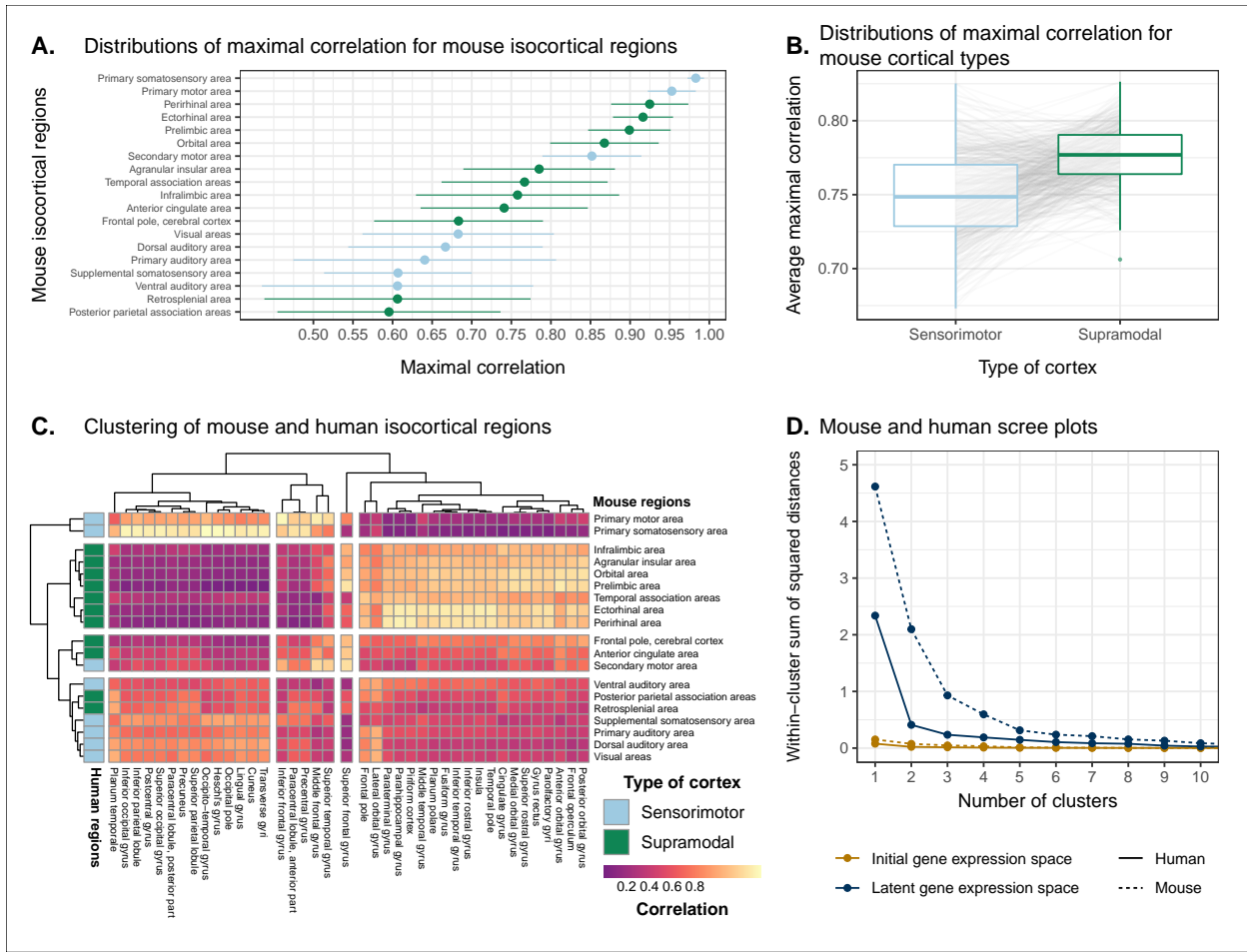


Figure 5-figure supplement 2. Similarity of mouse-human isocortical regions in latent spaces obtained using only cortical labels. (A) Maximal correlation distributions of mouse isocortical regions. Points and error bars represent mean and 95% confidence interval over latent space samples. (B) Distributions of average maximal correlation for sensorimotor and supramodal isocortical areas in each cortical latent space. Grey lines correspond to individual latent spaces. (C) Hierarchical clustering of mouse and human isocortical regions based on average latent space correlation values. Mouse regions are annotated as sensorimotor or supramodal. (D) Within-cluster sum of squared distances for different numbers of mouse and human isocortical clusters in the average cortical latent space and initial homologous gene space.

- 921 • Figure 2 - Source data 2: Correlations between mouse and human brain regions in all latent spaces (2
922 of 3).
- 923 • Figure 2 - Source data 3: Correlations between mouse and human brain regions in all latent spaces (3
924 of 3).
- 925 • Figure 3 - Source data 1: Scaled similarity profiles of the mouse primary motor area.
- 926 • Figure 3 - Source data 2: Ranks at a similarity of 0.75 for mouse regions in the homologous gene space
927 and all latent spaces.
- 928 • Figure 3 - Source data 3: Logistic regression model estimates for mouse regions.
- 929 • Figure 4 - Source data 1: Ranks of canonical neuroanatomical pairs for mouse regions in the homologous
930 gene space and all latent spaces.
- 931 • Figure 4 - Source data 2: Logistic regression model estimates for mouse regions.
- 932 • Figure 5 - Source data 1: Maximal correlations of mouse isocortical regions in all latent spaces.
- 933 • Figure 5 - Source data 2: Correlations between mouse and human isocortical regions in all latent
934 spaces.
- 935 • Figure 5 - Source data 3: Scree plot data.
- 936 • Figure 6 - Source data 1: Correlations between human striatal samples and mouse striatal targets in
937 all latent spaces.
- 938 • Figure 6 - Source data 2: Average latent space correlations of mouse striatal voxels with human regions.
- 939 • Figure 6 - Source data 3: Maximal correlations of mouse striatal voxels in all latent spaces (1 of 3).
- 940 • Figure 6 - Source data 4: Maximal correlations of mouse striatal voxels in all latent spaces (2 of 3).
- 941 • Figure 6 - Source data 5: Maximal correlations of mouse striatal voxels in all latent spaces (3 of 3).

942 **Supplementary files**

- 943 • Supplementary file 1: Biological modules enriched in the homologous gene set.